Supporting Information

Evidence for the "cocktail" nature of platinum-catalyzed alkyne and alkene hydrosilylation reactions

Evgeniia E. Ondar, Julia V. Burykina, Valentine P. Ananikov*

N.D. Zelinsky Institute of Organic Chemistry, Russian Academy of Sciences, Leninsky Prospect 47, Moscow, 119991, Russia

E-mail: val@ioc.ac.ru; http://AnanikovLab.ru

Table of contents

Hydrosilylation reaction conditions

Table S1. Reaction conditions of hydrosilylation of alkynes.

Alkyne / Silane	Phenylacetylene	1-Hexyne	Tolane	3-Hexyne	Trimethylsilyl acetylene
$HSiCl_3$	50°C / 5h / neat	50°C / 5h / neat	100°C / 9h / toluene	50°C / 4h / neat	40°C / 5h / neat
$HSiEt_3$	50°C / 8h / neat	80°C / 5h / neat	50°C / 8h / neat	80°C / 5h / neat	70°C / 5h / neat
$HSiPh_3$	70°C / 4h / neat	70°C / 4h / neat	90°C / 6h / neat	90°C / 8h / neat	70°C / 4h / neat

Pt_2dba_3 purity

The purity of the used $Pt_2dba_3 \cdot CHCl_3$ complex was determined by a previously described procedure.[1] Calculation of the purity was based on ^1H NMR characterization of the Pt_2dba_3 complex before catalyst preparation.

Electron microscopy study of the initial catalysts

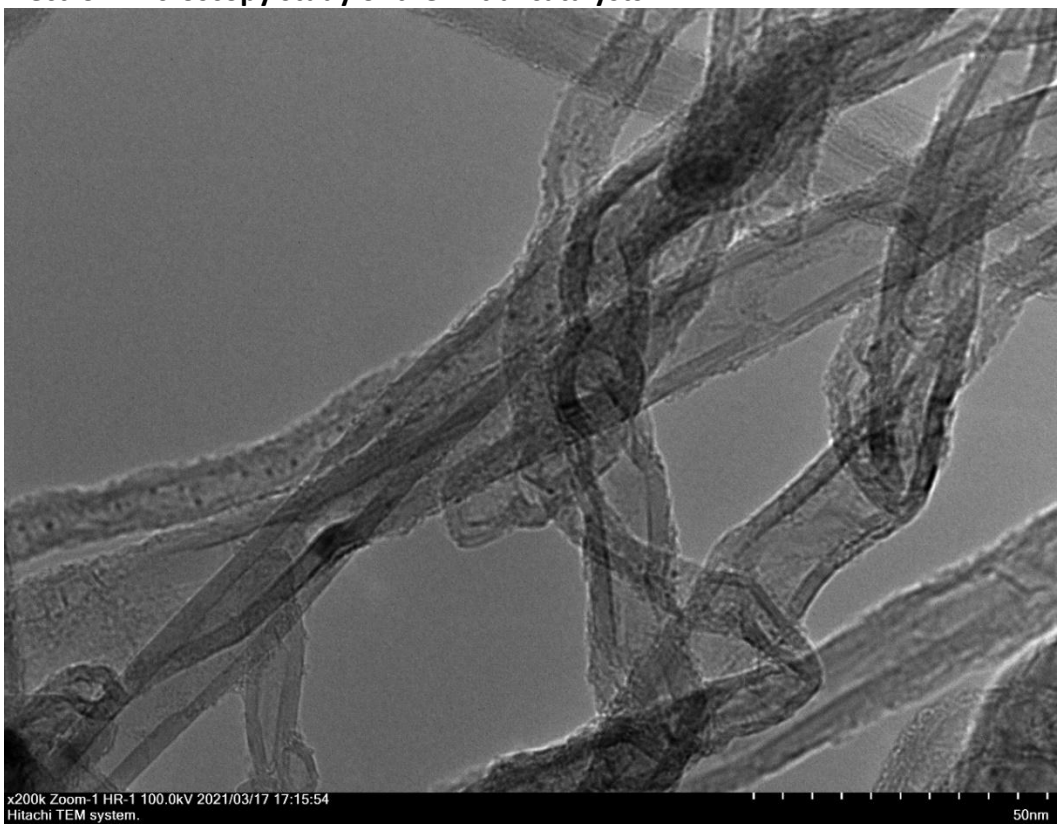

Figure S1. TEM images of initial Pt/MWCNT$_{chl}$ catalyst.

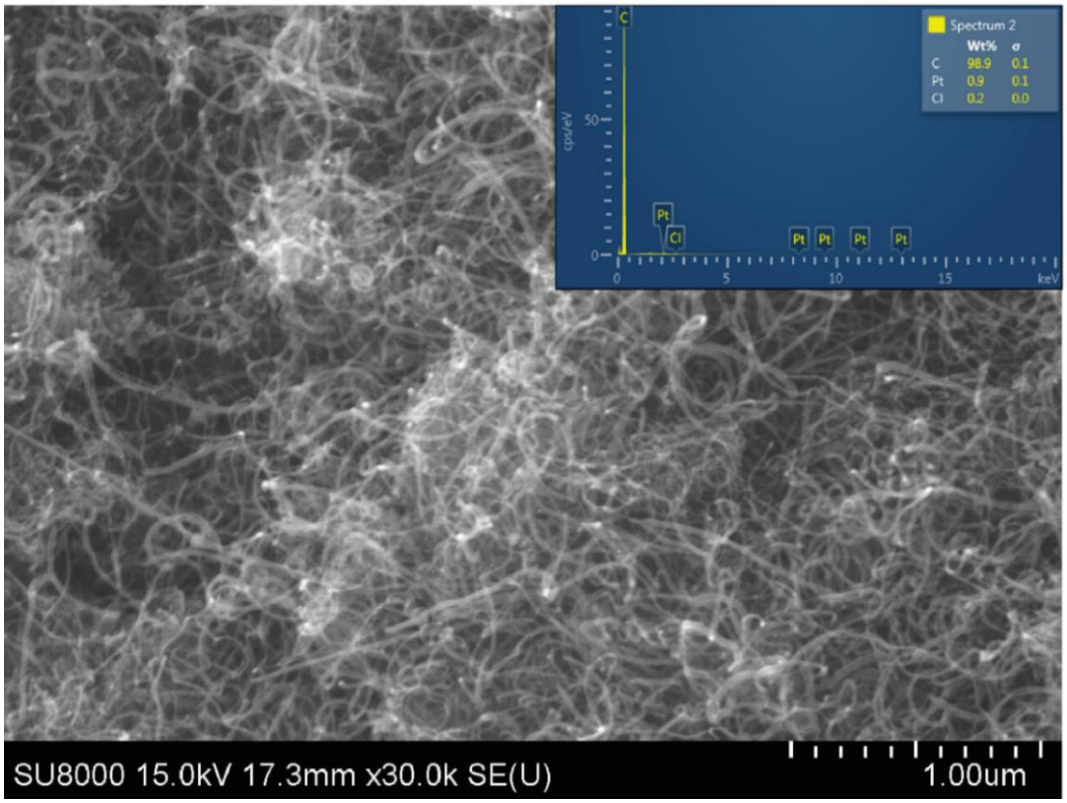

Figure S2. SEM/EDX of initial Pt/MWCNT$_{chl}$ catalyst.

Figure S3. TEM images of initial Pt/MWCNT$_{THF}$ catalyst**.**

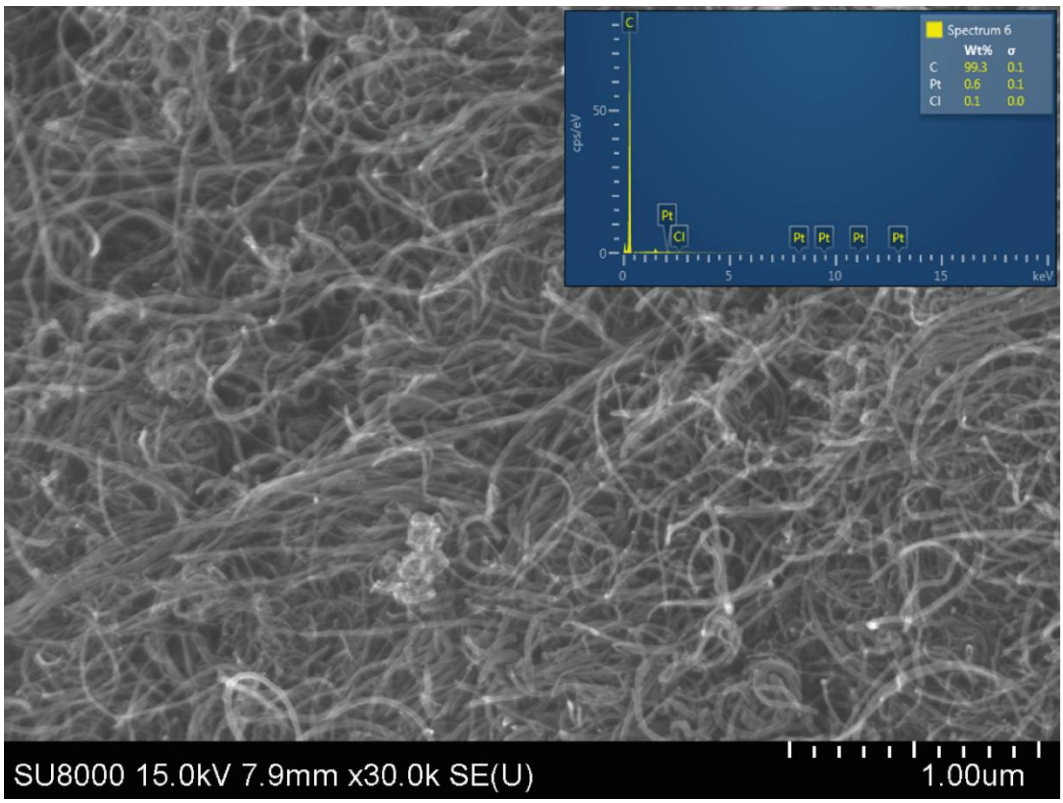

Figure S4. SEM/EDX of initial Pt/MWCNT$_{THF}$ catalyst.

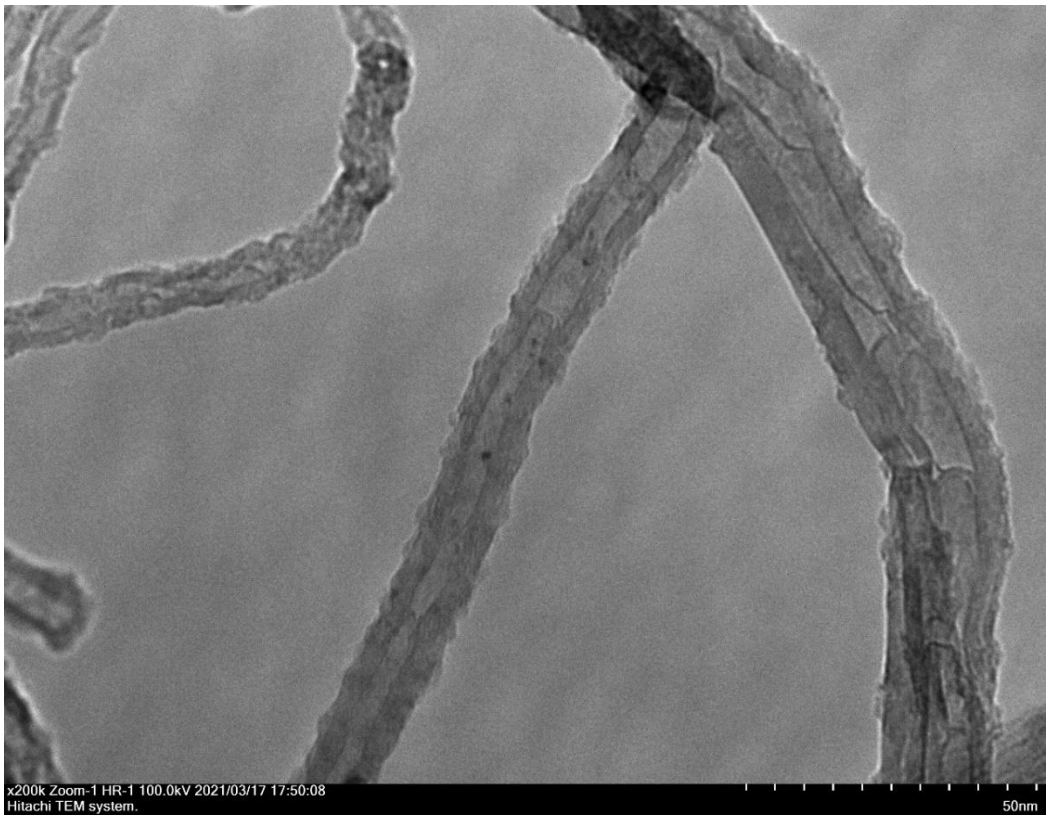

Figure S5. TEM images of initial Pt/MWCNT$_{tol}$ catalyst**.**

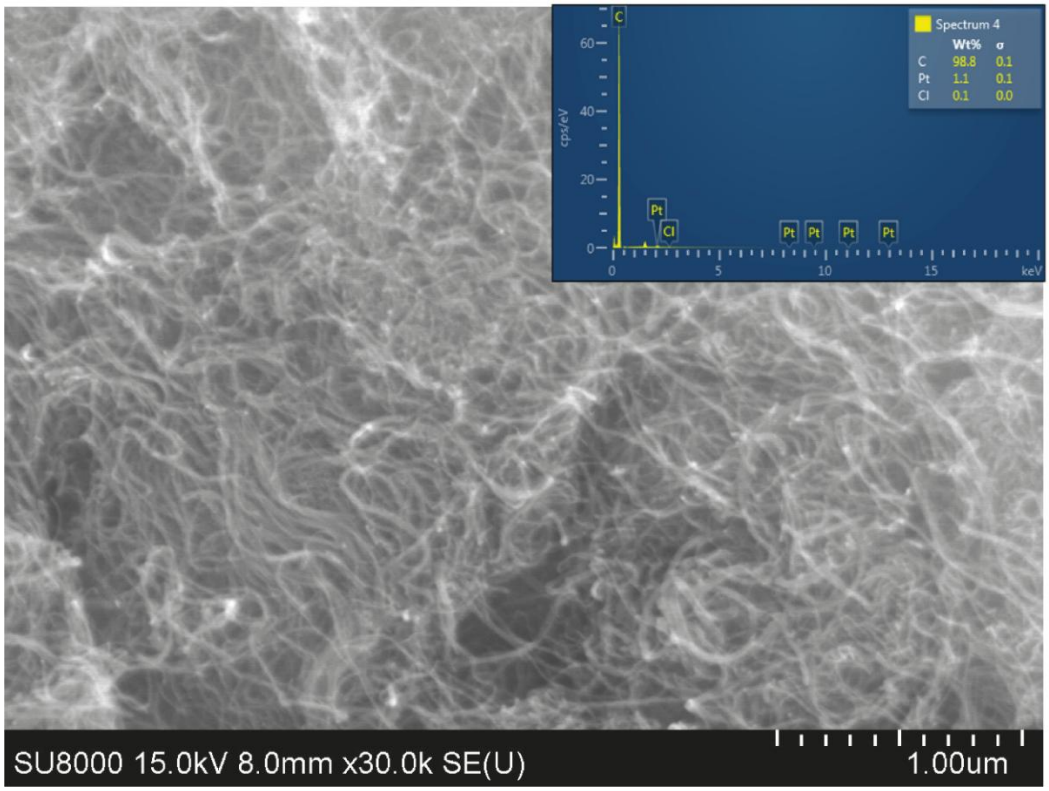

Figure S6. SEM/EDX of initial Pt/MWCNT$_{tol}$ catalyst.

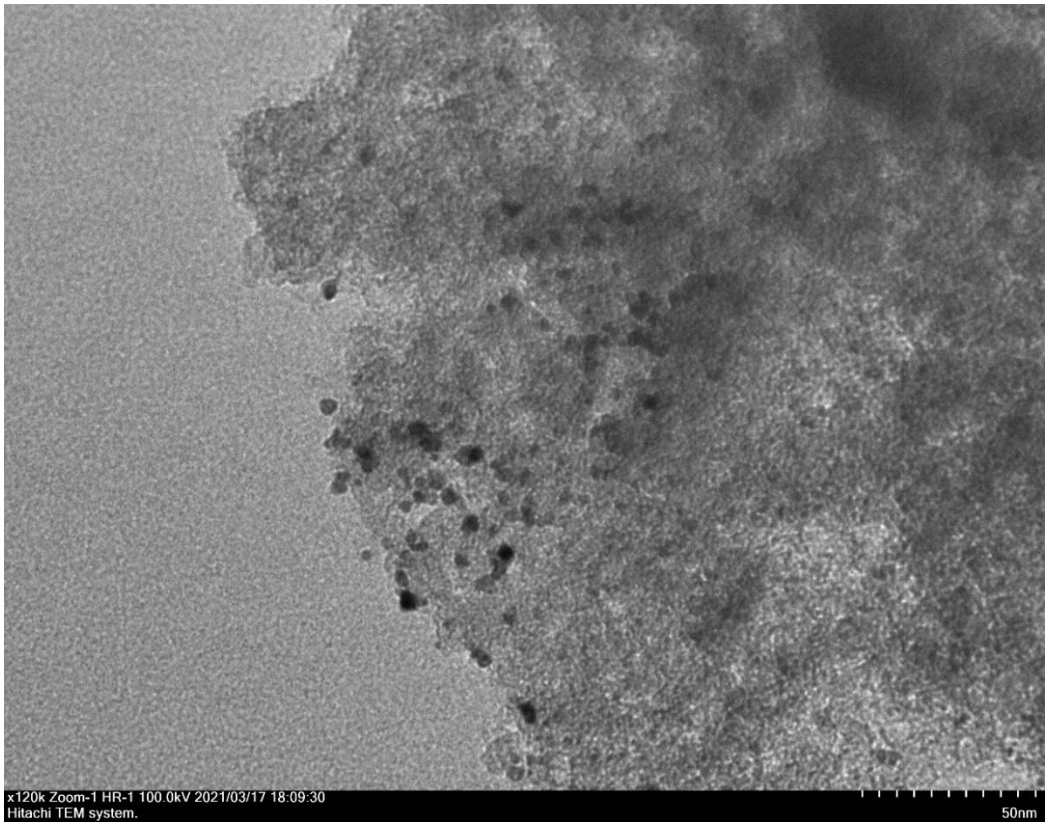

Figure S7. TEM images of initial Pt/C catalyst.

Leaching in solvent

0.3 wt. % Pt/MWCNT$_{chl}$, Pt/MWCNT$_{THF}$, Pt/MWCNT$_{tol}$ and commercial 1 wt. % Pt/C were refluxed for 1 h in THF and analyzed by ESI-HRMS and TEM. Two points were taken into consideration – initial and 1 h points.

Table S2. ESI-HRMS leaching study of Pt/MWCNT$_{chl}$, Pt/MWCNT$_{THF}$, Pt/MWCNT$_{tol}$ catalysts.[a]

Entry	Time point	Pt/C	Pt/MWCNT$_{chl}$	Pt/MWCNT$_{THF}$	Pt/MWCNT$_{tol}$
1	initial	-	$[PtCl_3(dba)(N_2)_2]^-$	-	-
2	1 hour	-	$[PtCl_3]^-$ $[PtCl_2NO_2]^-$ $[PtCl_3(dba)(N_2)_2]^-$ $[PtCl_3(dba)]^-$	$[PtCl_2NO_2]^-$ $[PtCl_3(dba)(N_2)_2]^-$	$[PtCl_3]^-$ $[PtCl_3(dba)NO_2]^-$ $[PtCl_3(dba)(N_2)_2]^-$ $[PtCl_3(dba)]^-$

[a] ESI-HRMS study of Pt molecular complexes present in the solution at the beginning of the experiment and after 1 h, respectively.

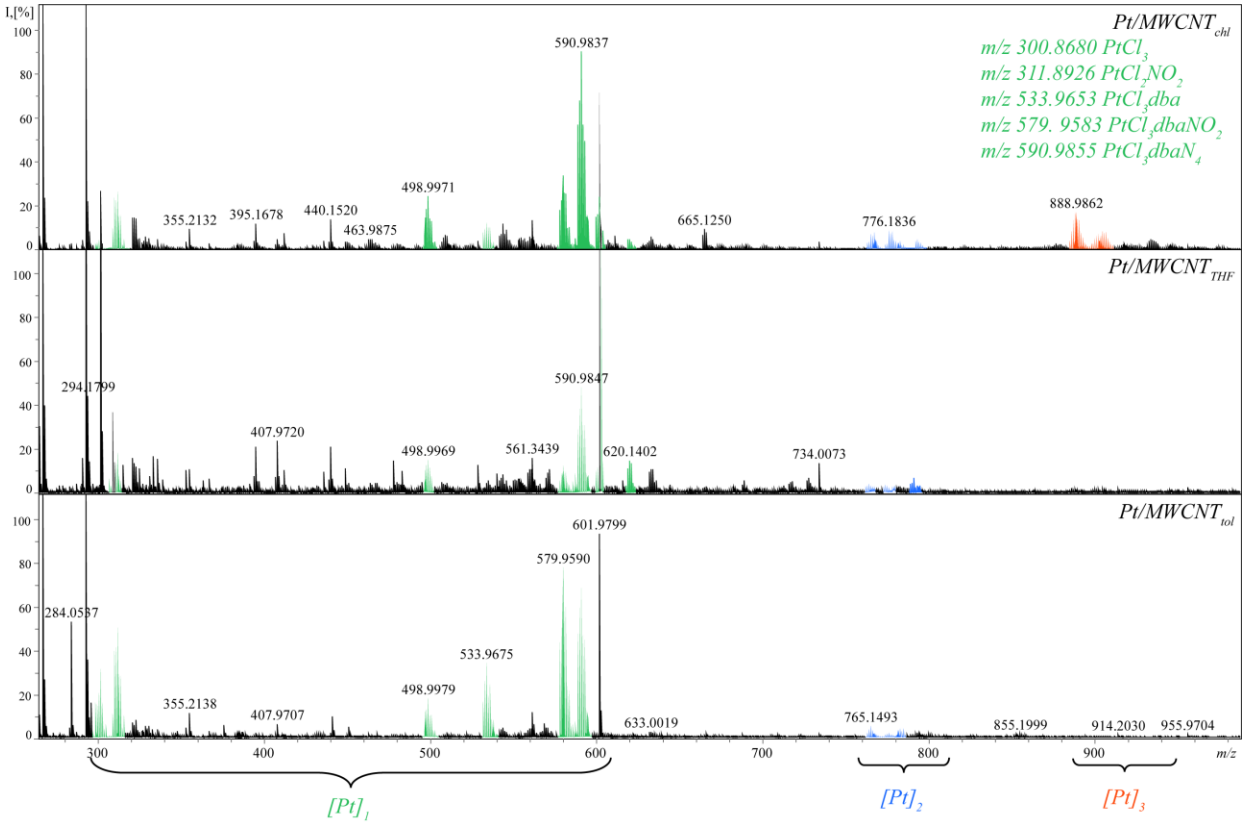

Figure. S8. ESI-HRMS spectra of Pt/MWCNT$_{chl}$, Pt/MWCNT$_{THF}$, Pt/MWCNT$_{tol}$ in THF after 1 h of reflux. Complexes with one platinum atom are colored green, with two Pt atoms in blue and three atoms in orange.

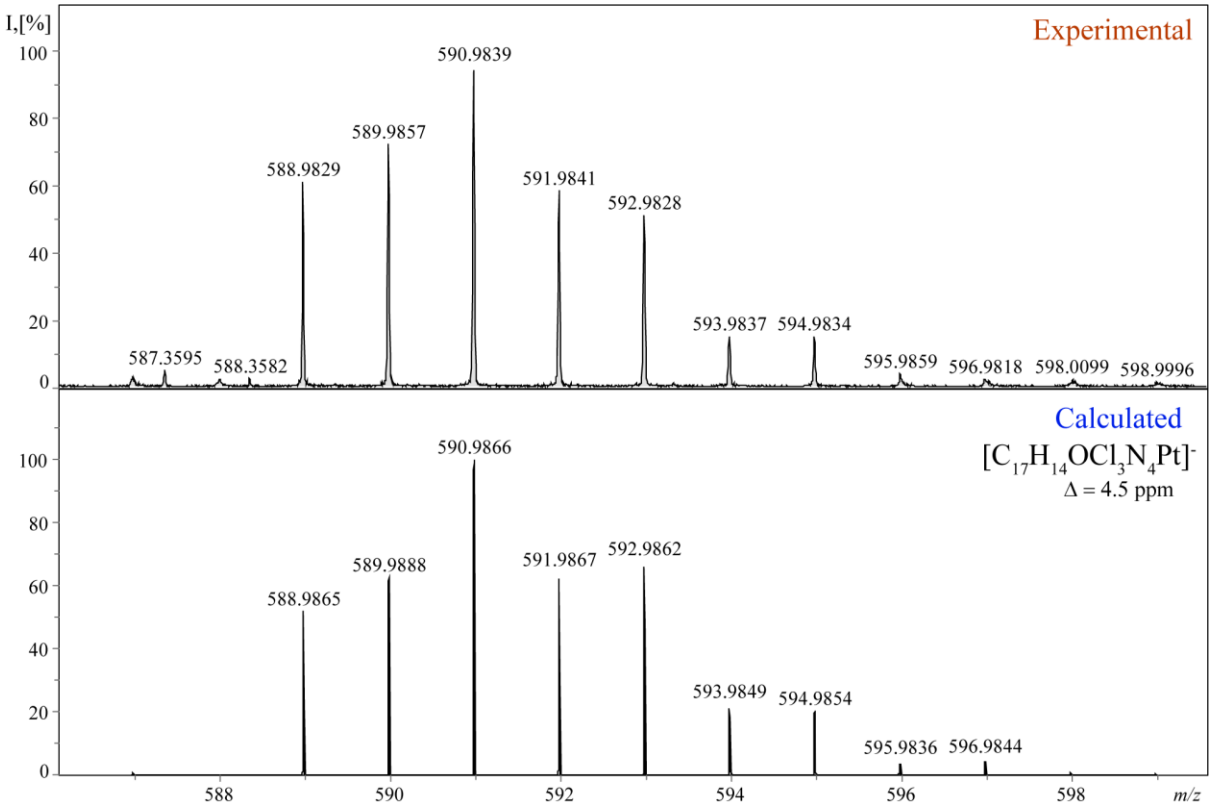

Figure S9. Experimentally detected and theoretical ESI-(-)HRMS spectrum of Pt/MWCNT$_{chl}$/THF/1h; main experimental peak $[M]^-$ = 590.9839 Da, calculated for $[C_{17}H_{14}OCl_3N_4Pt]$ = 590.9866 Da, Δ = 4.5 ppm.

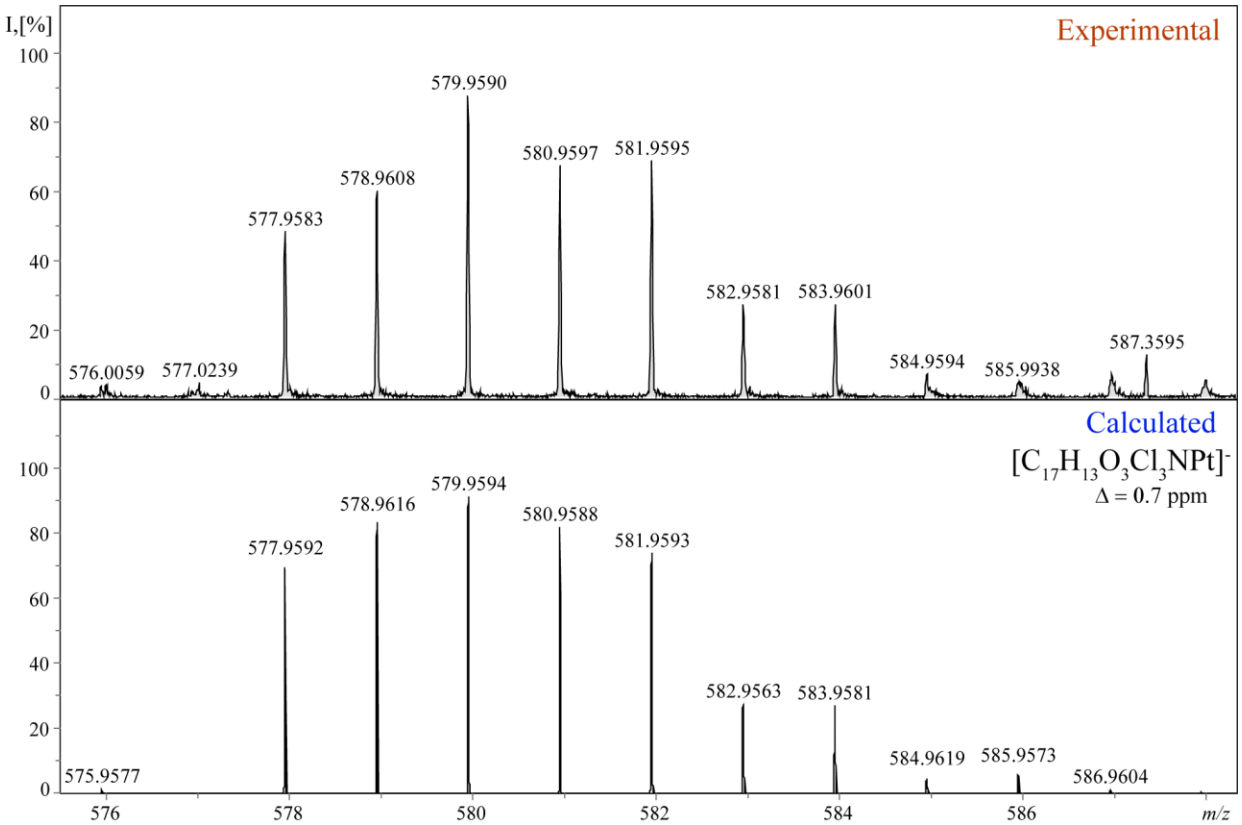

Figure S10. Experimentally detected and theoretical ESI-(-)HRMS spectra of Pt/MWCNT$_{chl}$/THF/1h; main experimental peak $[M-H]^-$ = 579.9590 Da, calculated for $[C_{17}H_{13}O_3Cl_3NPt]$ = 579.9594 Da, Δ = 0.7 ppm.

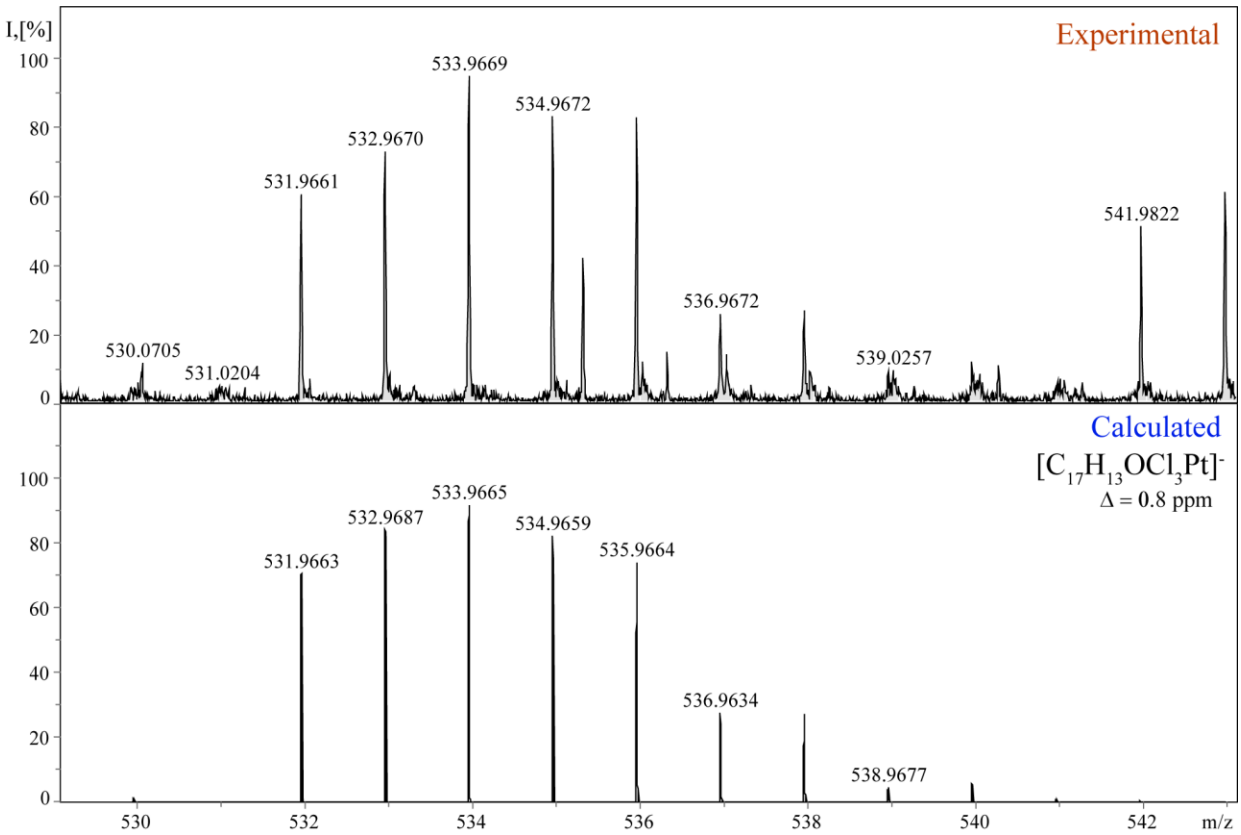

Figure S11. Experimentally detected and theoretical ESI-(-)HRMS spectra of Pt/MWCNT$_{chl}$/THF/1h; main experimental peak $[M\text{-}H]^-$ = 533.9669 Da, calculated for $[C_{17}H_{13}OCl_3Pt]$ = 533.9665 Da, Δ = 0.8 ppm.

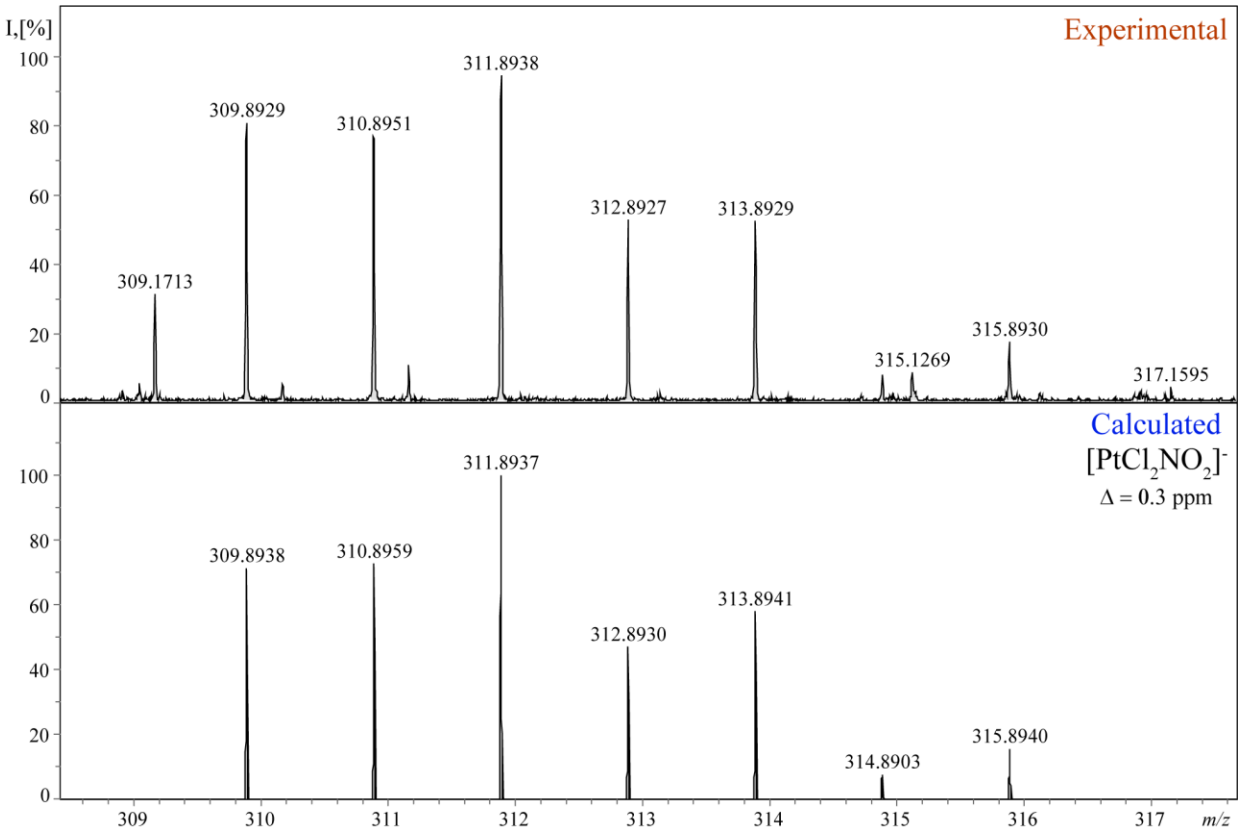

Figure S12. Experimentally detected and theoretical ESI-(-)HRMS spectra of Pt/MWCNT$_{chl}$/THF/1h; main experimental peak $[M]^-$ = 311.8938 Da, calculated for $[PtCl_2NO_2]$ = 311.8937 Da, Δ = 0.3 ppm.

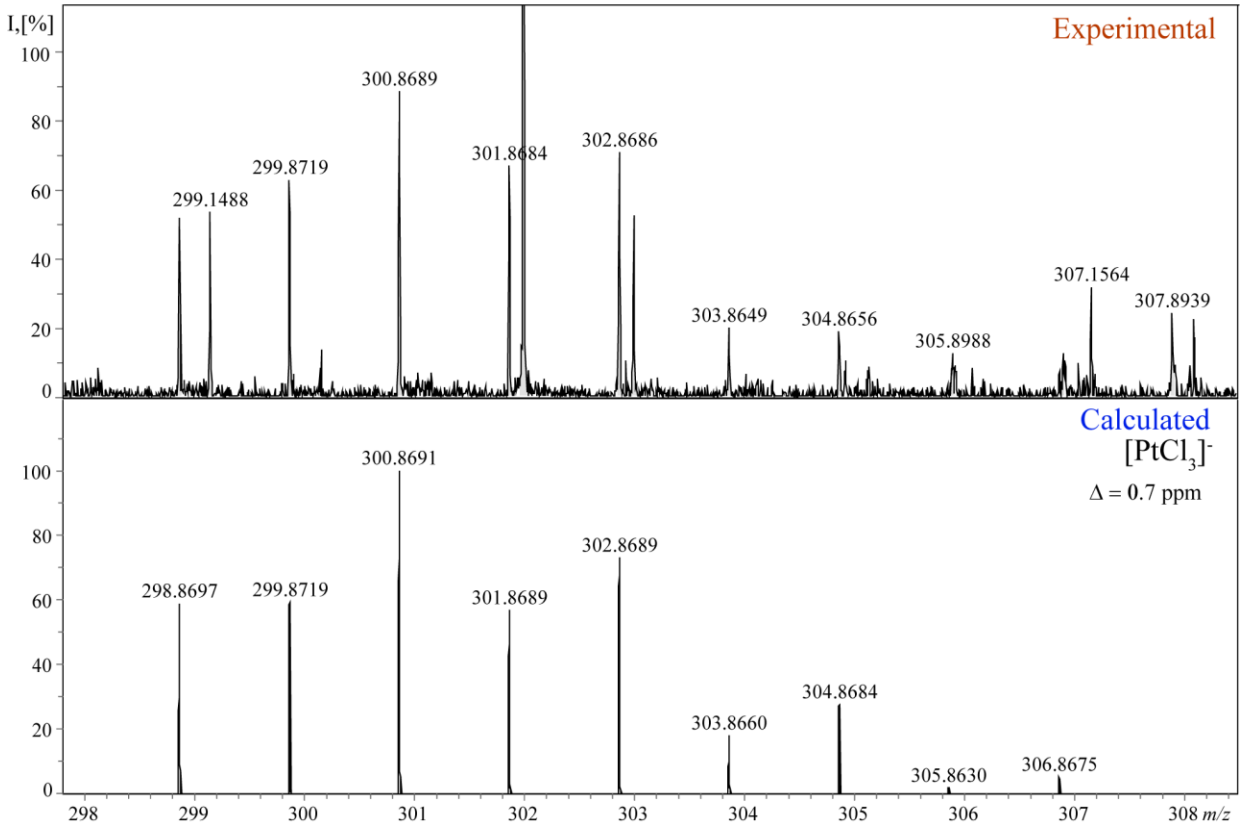

Figure S13. Experimentally detected and theoretical ESI-(-)HRMS spectra of Pt/MWCNT$_{chl}$/THF/1h; main experimental peak $[M]^-$ = 300.8689 Da, calculated for $[PtCl_3]$ = 300.8691 Da, Δ = 0.7 ppm.

Table S3. Pt NPs size confidence intervals before and 1 h after the experiment.

Entry	Precatalyst	Initial Pt NPs size, nm[a]	Pt NPs size after treatment, nm[b]
1	Pt/C	3.9 ± 1.0	3.3 ± 1.3
2	Pt/MWCNT$_{chl}$	2.1 ± 0.6	1.9 ± 0.5
3	Pt/MWCNT$_{THF}$	2.2 ± 0.2	2.0 ± 0.7
4	Pt/MWCNT$_{tol}$	2.1 ± 0.6	1.6 ± 0.5

[a] Pt NPs size on the surface of the initial catalysts before the leaching experiment; [b] Pt NPs size on the surface of the catalysts after 1 h of treatment.

ESI-HRMS online monitoring of model reaction

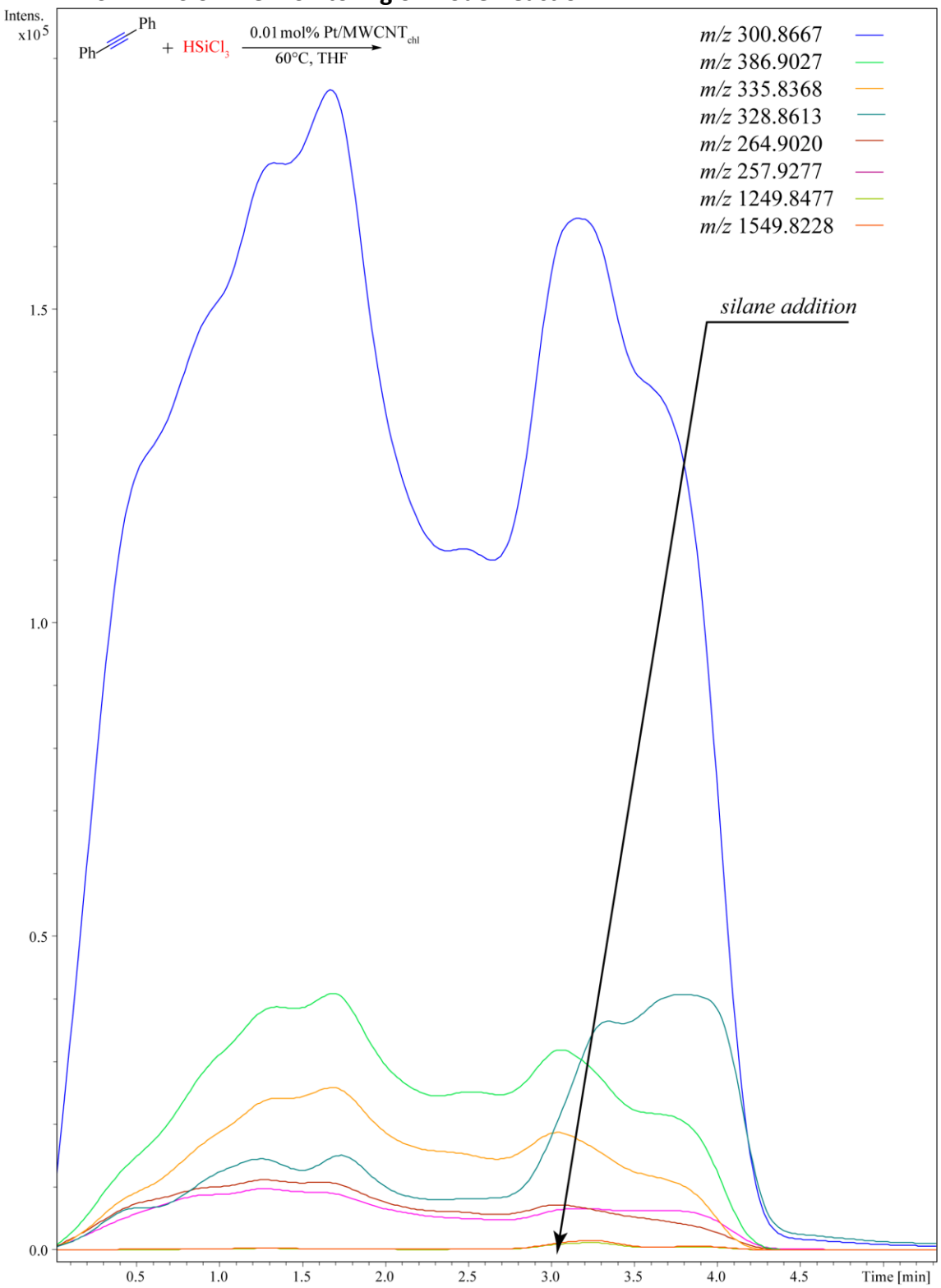

Figure. S14. Gauss-smoothed curves (3 sec, 5 cycles) for the real-time abundances of ions in tolane (**1a**) and trichlorosilane (**2a**) reaction catalysed by Pt/MWCNT$_{chl}$.

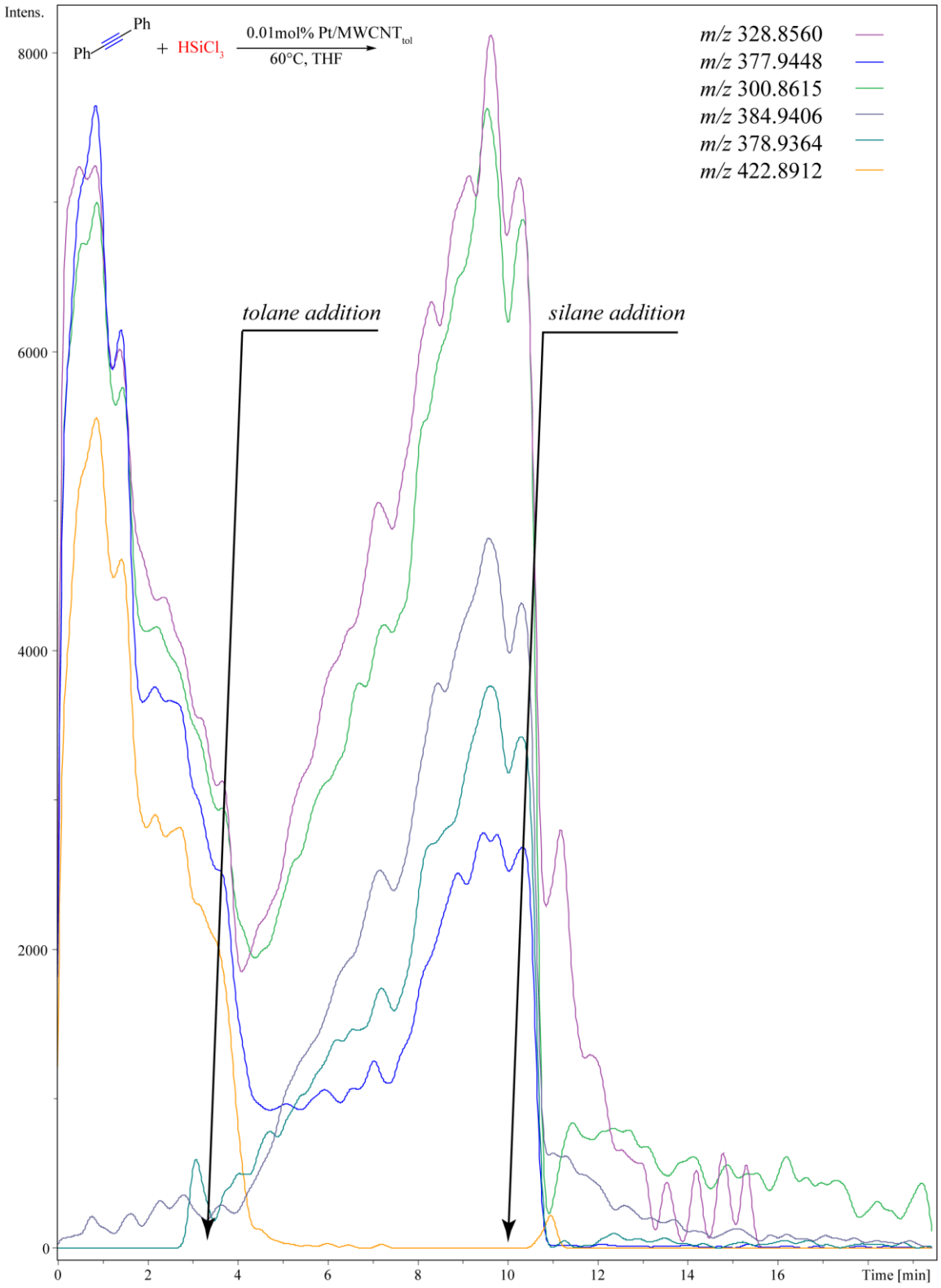

Figure. S15. Gauss-smoothed curves (3 sec, 5 cycles) for the real-time abundances of ions in tolane (**1a**) and trichlorosilane (**2a**) reaction-catalysed Pt/$MWCNT_{tol}$.

ESI-HRMS spectra of the allyl bromide hydrosilylation reaction mixture

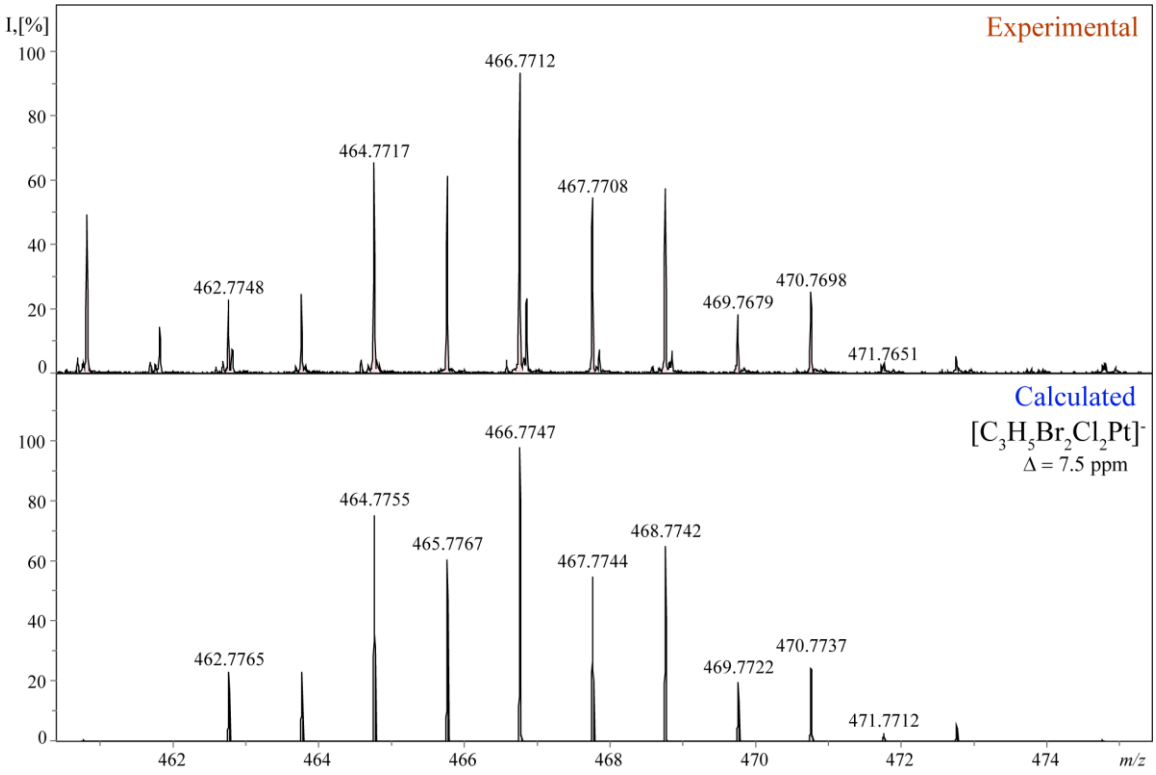

Figure S16. Experimentally detected and theoretical ESI-(-)HRMS spectra of Pt/MWCNT$_{THF}$/THF/5h; main experimental peak $[M]^-$ = 466.7712 Da, calculated for $[C_3H_5PtBr_2Cl_2]$ = 466.7747 Da, Δ = 7.5 ppm.

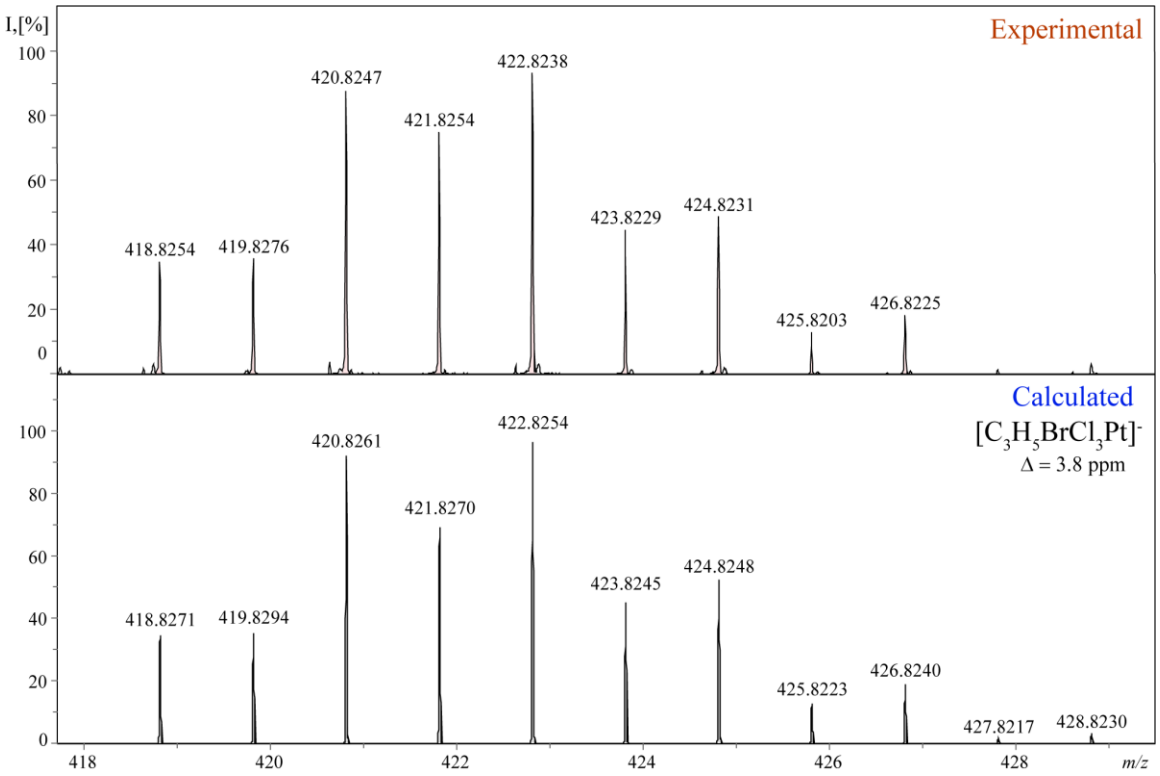

Figure S17. Experimentally detected and theoretical ESI-(-)HRMS spectra of Pt/MWCNT$_{THF}$/THF/5h; main experimental peak $[M]^-$ = 422.8238 Da, calculated for $[C_3H_5PtBrCl_3]$ = 422.8254 Da, Δ = 3.8 ppm.

Capture of metal clusters in solution using the “nanofishing” procedure

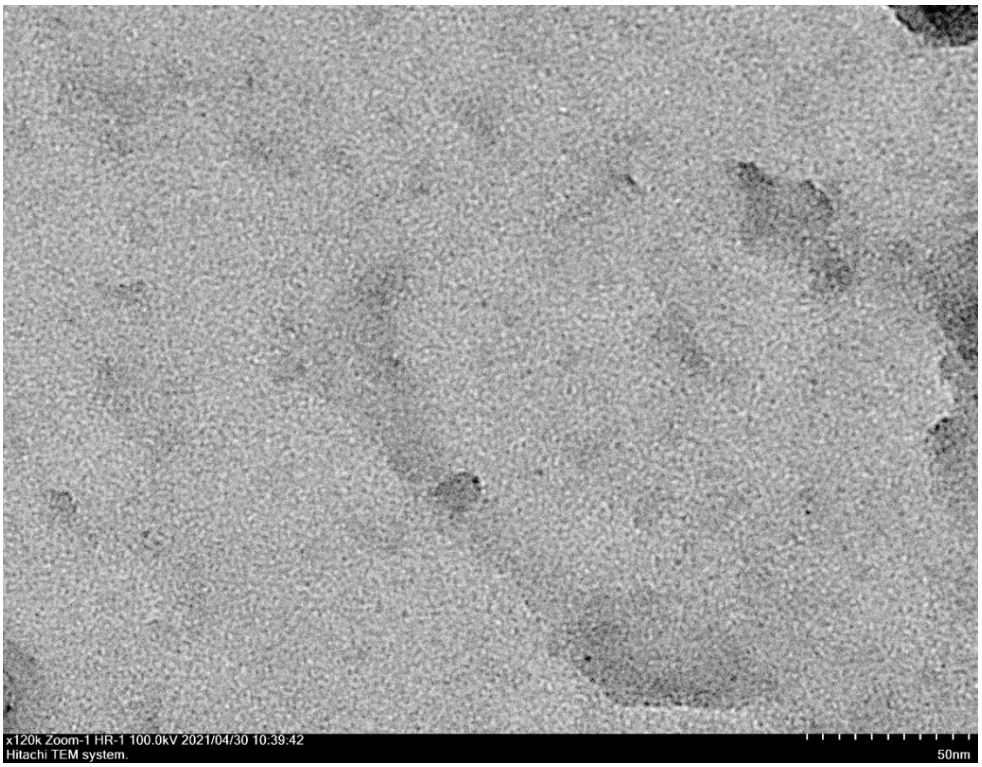

Figure S18. TEM image of Pt NPs from $HSiCl_3$ (**2a**) and Ph_2C_2 (**1a**) reaction supernatant in the presence of $Pt/MWCNT_{chl}$.

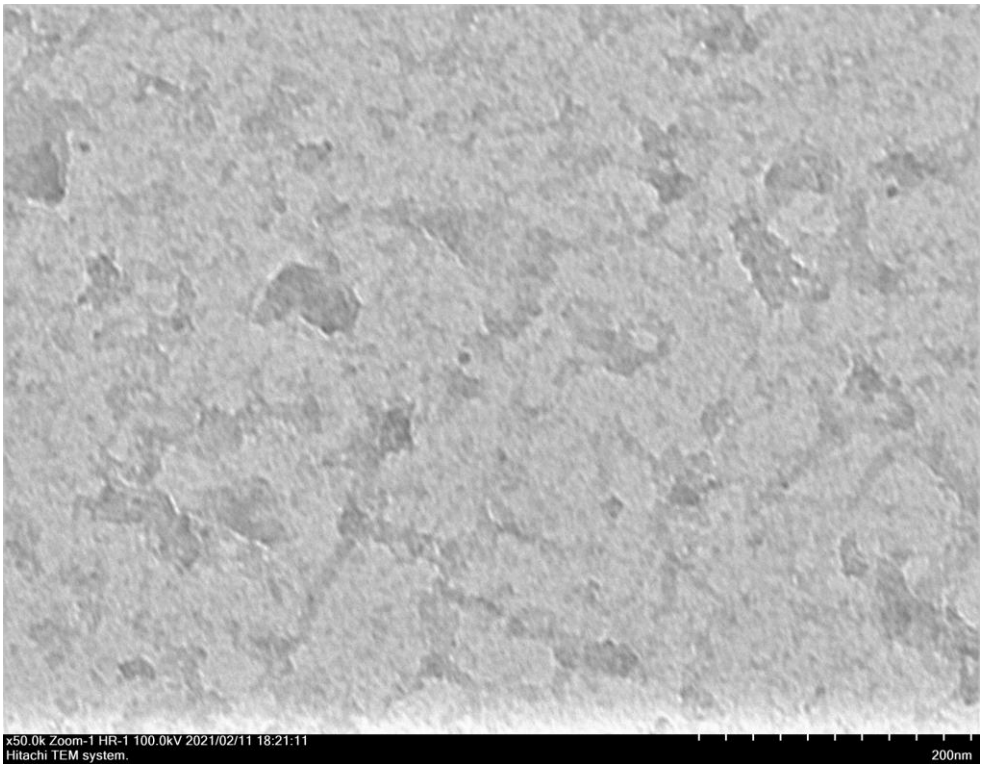

Figure S19. TEM image of Pt NPs from $HSiCl_3$ (**2a**) and Ph_2C_2 (**1a**) reaction supernatant in the presence of $Pt/MWCNT_{THF}$.

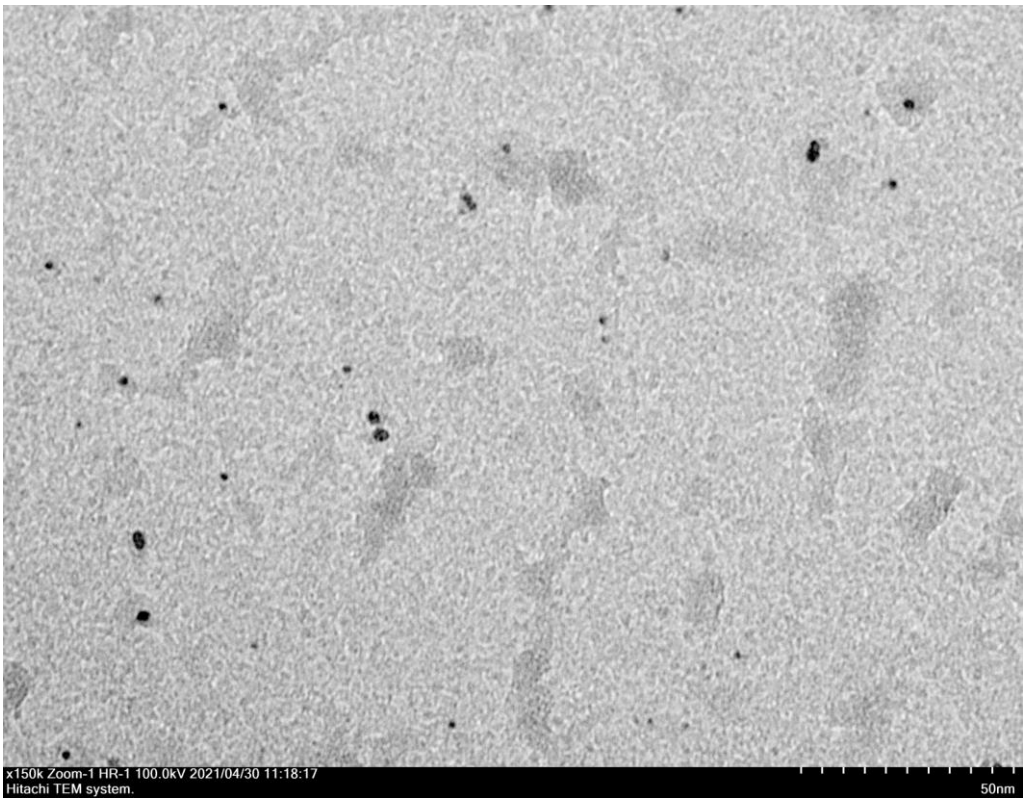

Figure S20. TEM image of Pt NPs from $HSiCl_3$ (**2a**) and Ph_2C_2 (**1a**) reaction supernatant in the presence of $Pt/MWCNT_{tol}$**.**

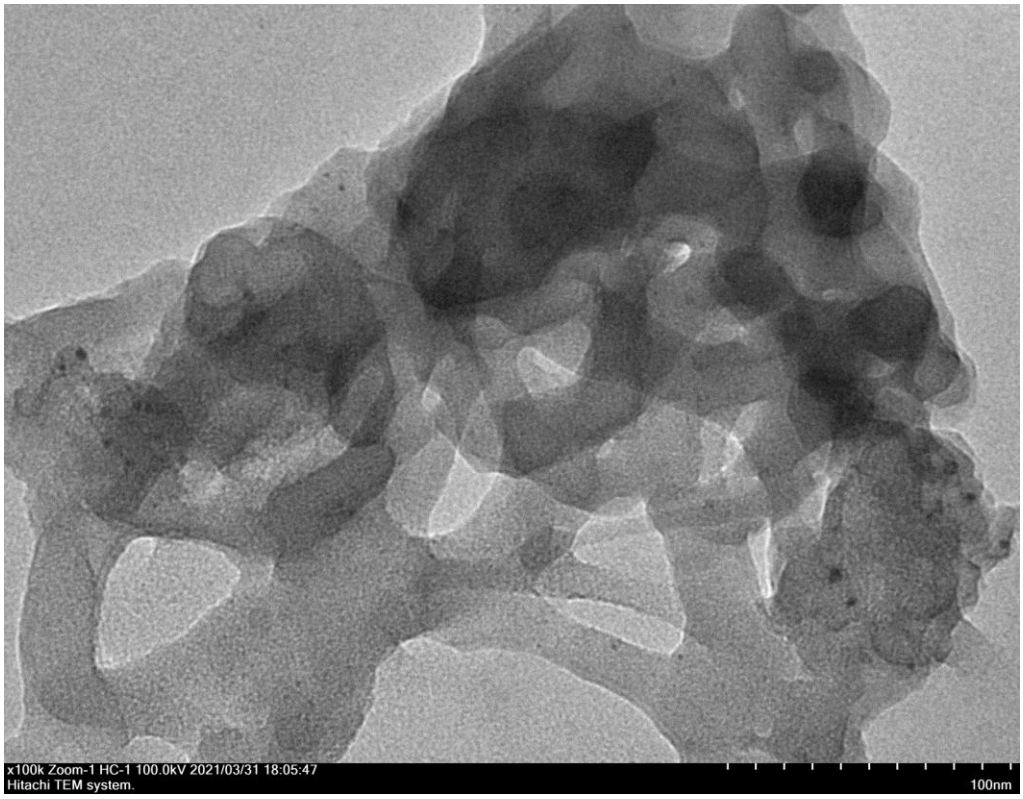

Figure S21. TEM image of Pt NPs from $HSiCl_3$ (**2a**) and Ph_2C_2 (**1a**) reaction supernatant in the presence of Pt/C**.**

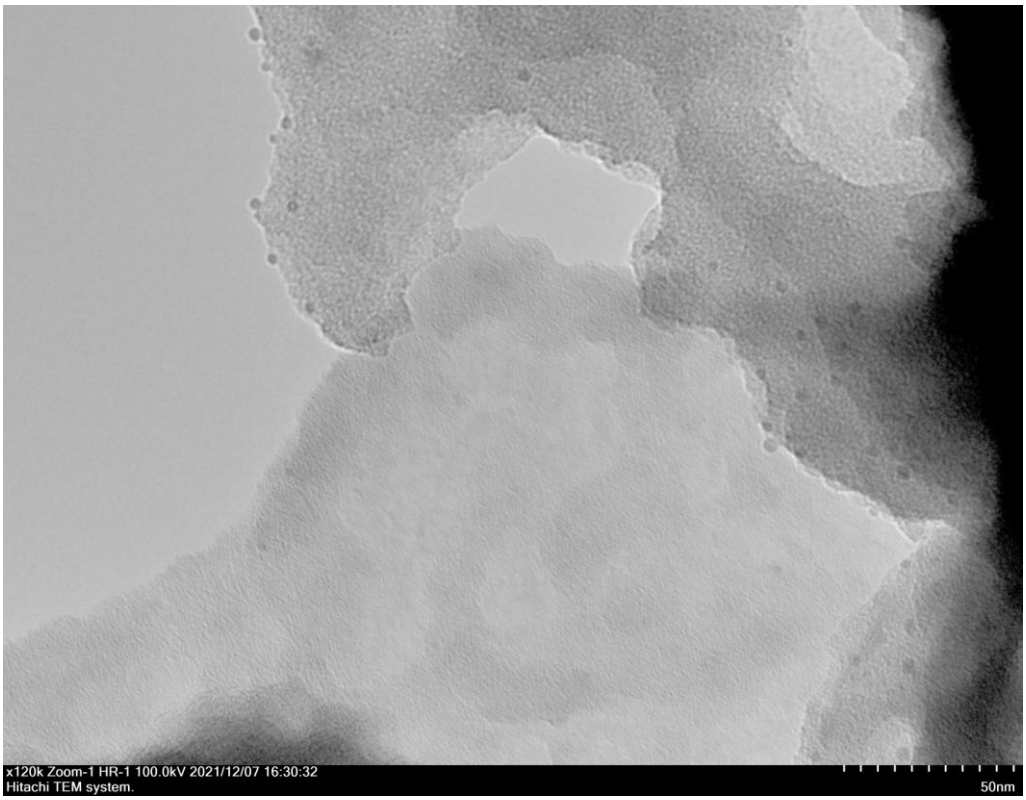

Figure S22. TEM image of Pt NPs from $HSiCl_3$ (**2a**) and allyl bromide reaction supernatant in the presence of Pt/C**.**

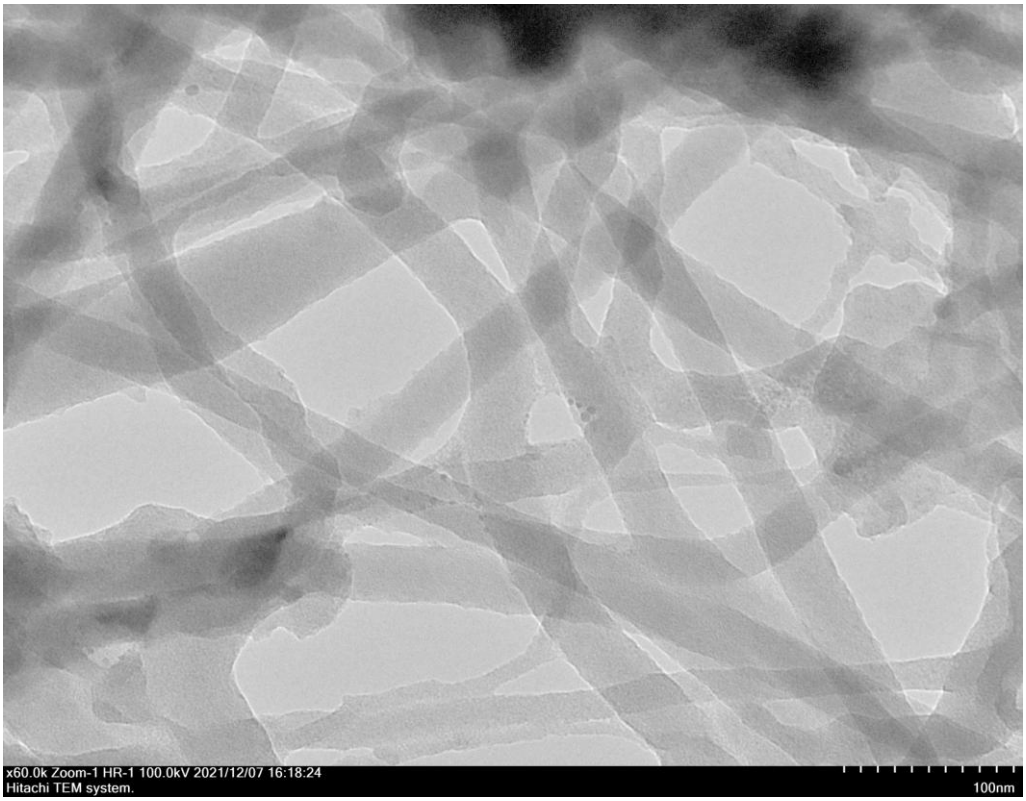

Figure S23. TEM image of Pt NPs from $HSiCl_3$ (**2a**) and allyl bromide reaction supernatant in the presence of $Pt/MWCNT_{THF}$**.**

Capture of metal clusters in solution using Fairlamb's method

The Fairlamb's method[2] was provided to check the aggregation of Pt particles in the supernatant. The model reaction was carried out in the presence of $Pt/MWCNT_{chl}$, and the reaction mixture was filtered by using a PTFE membrane with a pore size of 0.45 μm. 20 mg of PVP (polyvinylpirrolidone, mol. wt. 40000) was added into 1 ml of the supernatant. The precipitate was sampled on the TEM grid and washed with ethanol. The grid was examined by use of TEM.

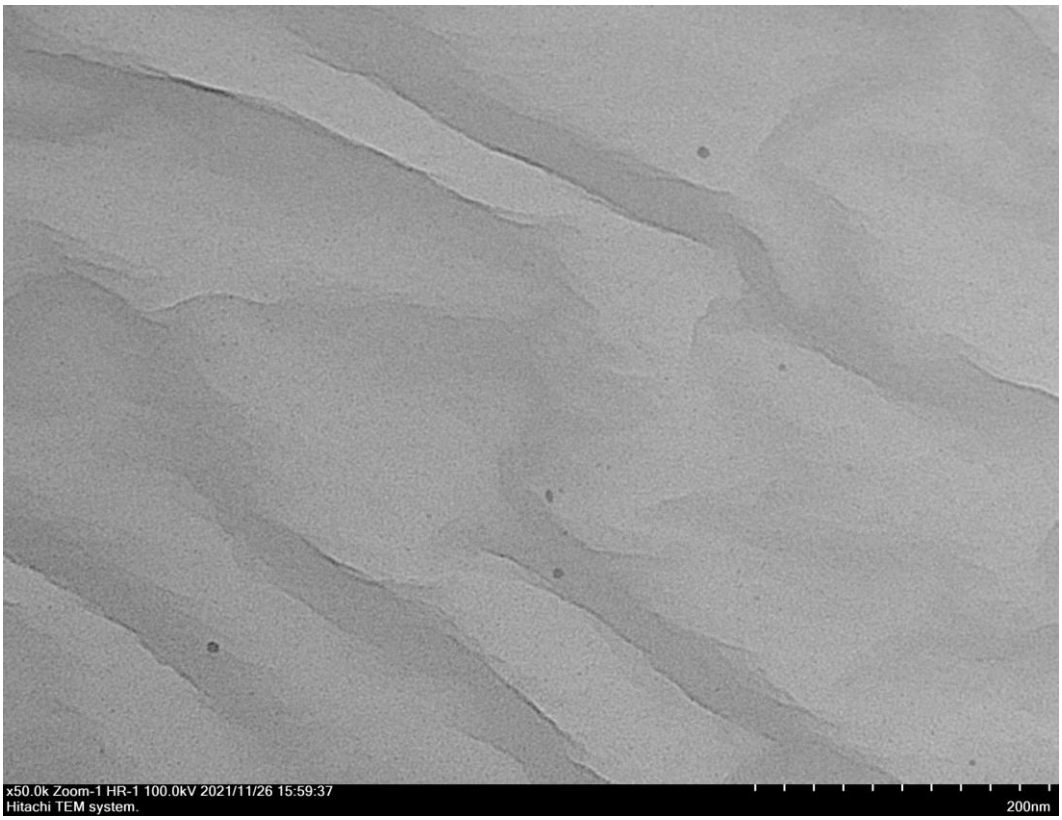

Figure S24. TEM image of Pt NPs from $HSiCl_3$ (**2a**) and Ph_2C_2 (**1a**) reaction solution in the presence of $Pt/MWCNT_{chl}$ by use of PVP (polyvinylpyrrolidone).

Electron microscopy study of the catalysts isolated after the reaction

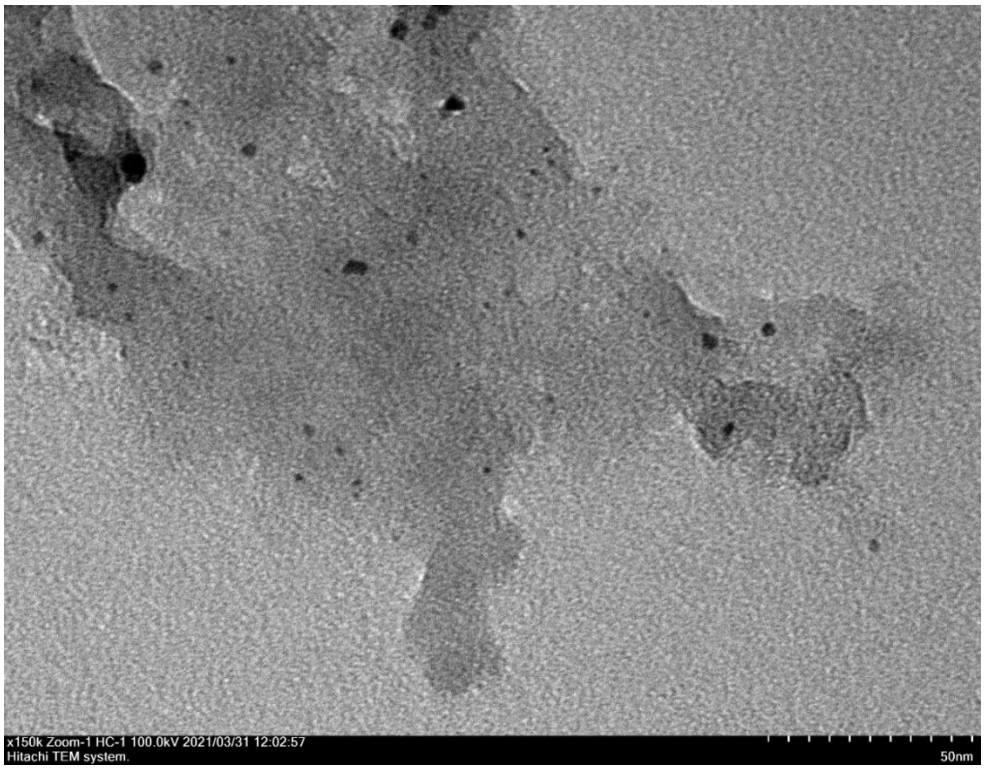

Figure S25. TEM images of Pt nanoparticles of Pt/C after the model reaction.

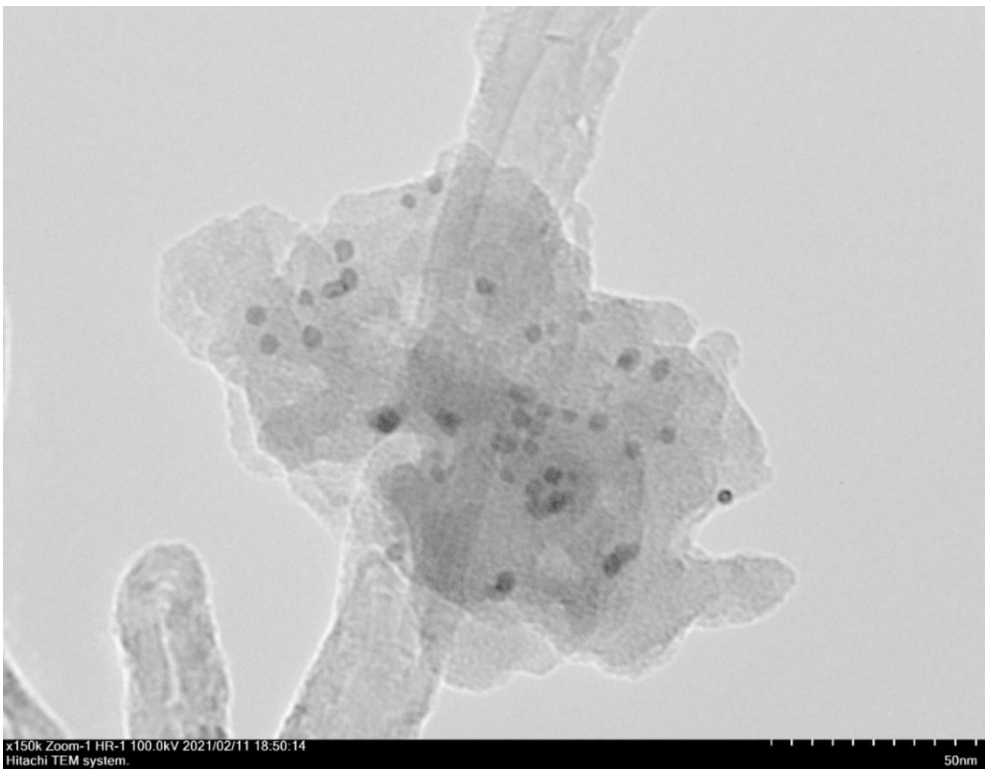

Figure S26. TEM images of Pt nanoparticles of Pt/MWCNT$_{chl}$ after the model reaction.

Figure S27. TEM images of Pt nanoparticles of Pt/MWCNT$_{THF}$ after the model reaction.

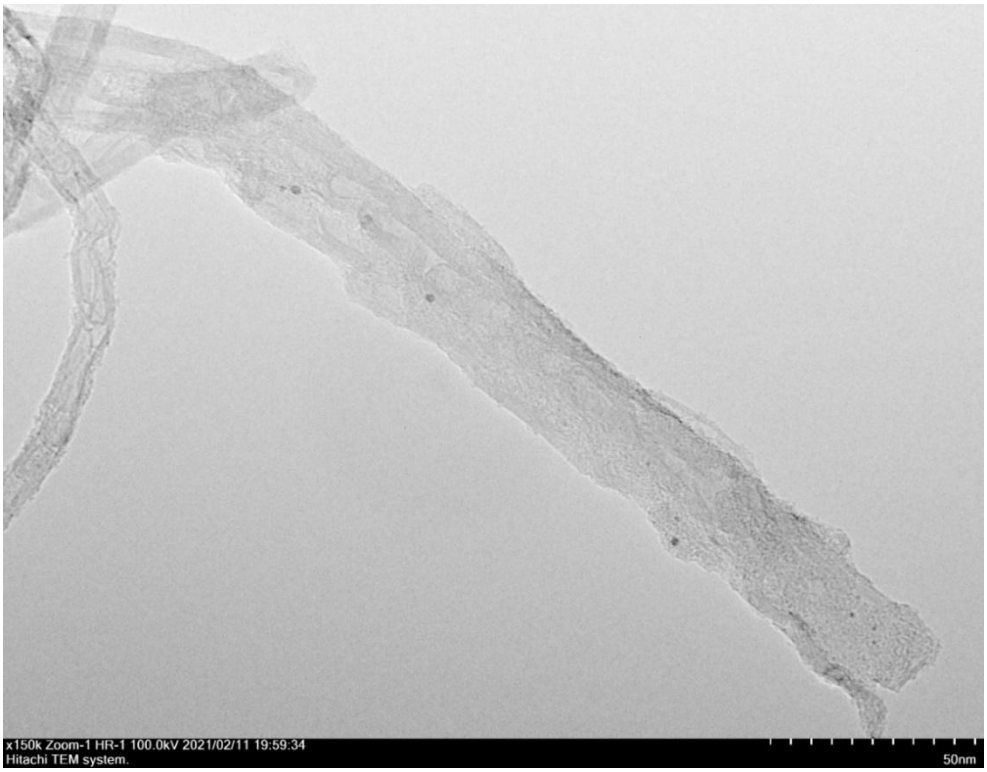

Figure S28. TEM images of Pt nanoparticles of Pt/MWCNT$_{tol}$ after the model reaction.

Figure S29. TEM images of Pt nanoparticles of Pt/MWCNT$_{THF}$ after allyl bromide hydrosilylation by $HSiCl_3$.

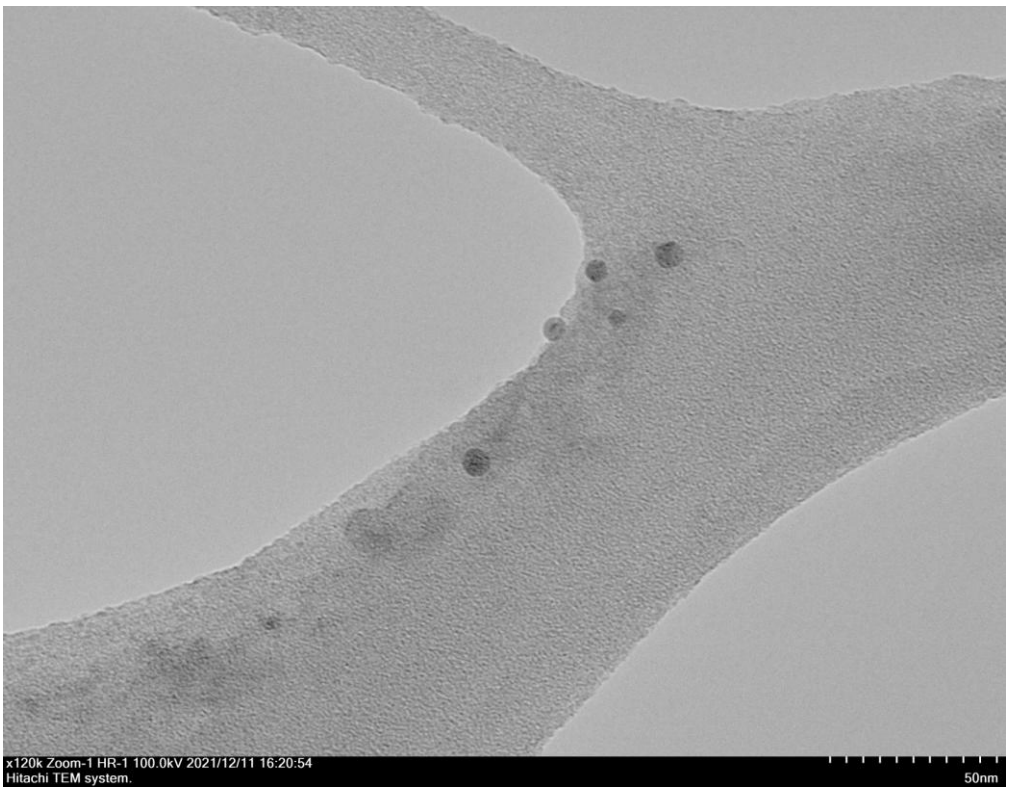

Figure S30. TEM images of Pt nanoparticles of Pt/C after allyl bromide hydrosilylation by $HSiCl_3$.

Electron microscopy study of Pt/MWCNT$_{THF}$ and Pt/C catalysts isolated after reactions with silane variation

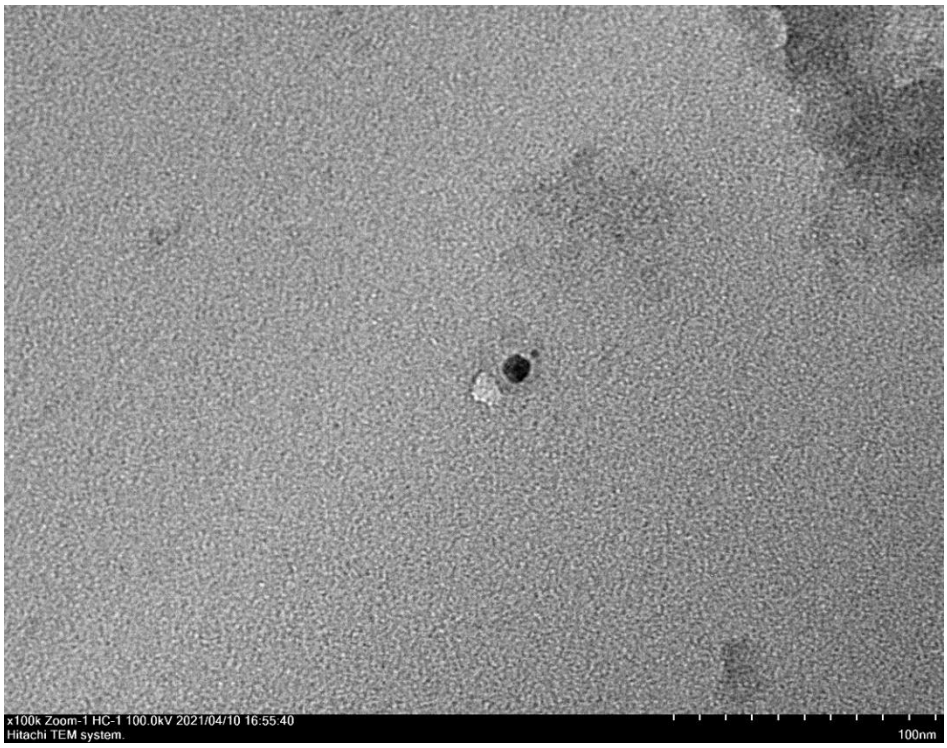

Figure S31. TEM image of Pt NPs from $HSiCl_3$ (**2a**) and Ph_2C_2 (**1a**) reaction supernatant in the presence of Pt/MWCNT$_{THF}$.

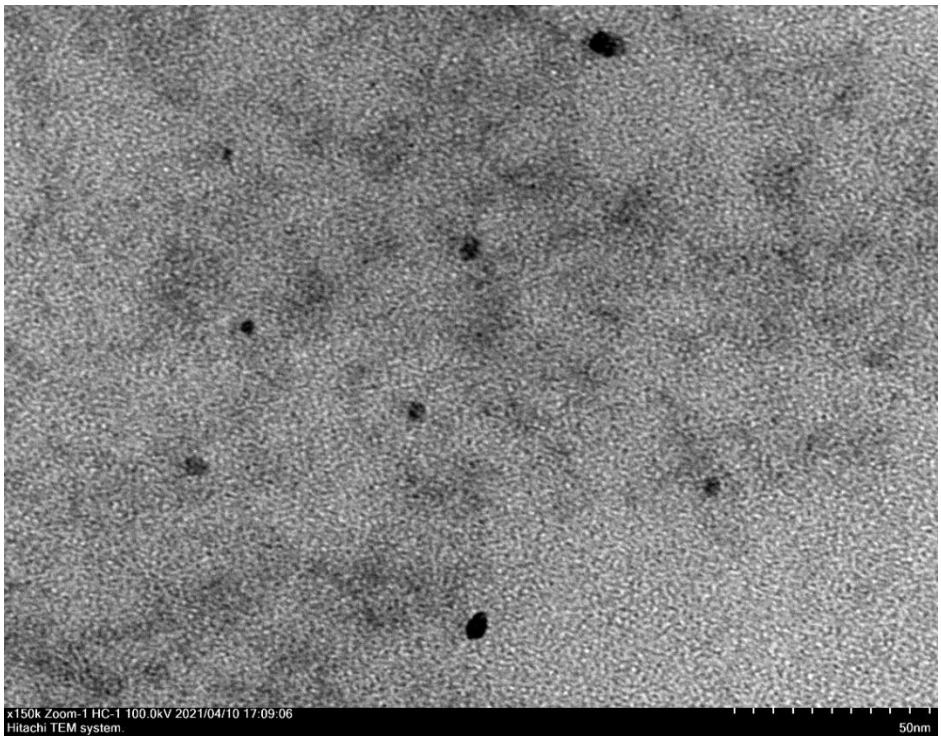

Figure S32. TEM image of Pt NPs from $HSiEt_3$ (**2b**) and Ph_2C_2 (**1a**) reaction supernatant in the presence of Pt/MWCNT$_{THF}$.

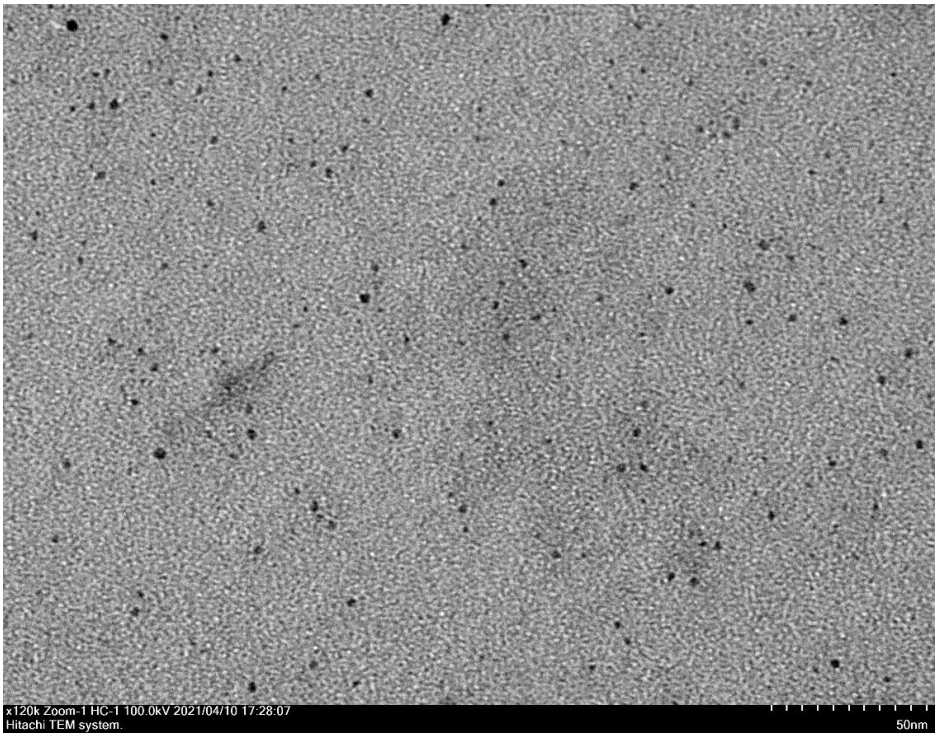

Figure S33. TEM image of Pt NPs from $HSiPh_3$ (**2c**) and Ph_2C_2 (**1a**) reaction supernatant in the presence of $Pt/MWCNT_{THF}$.

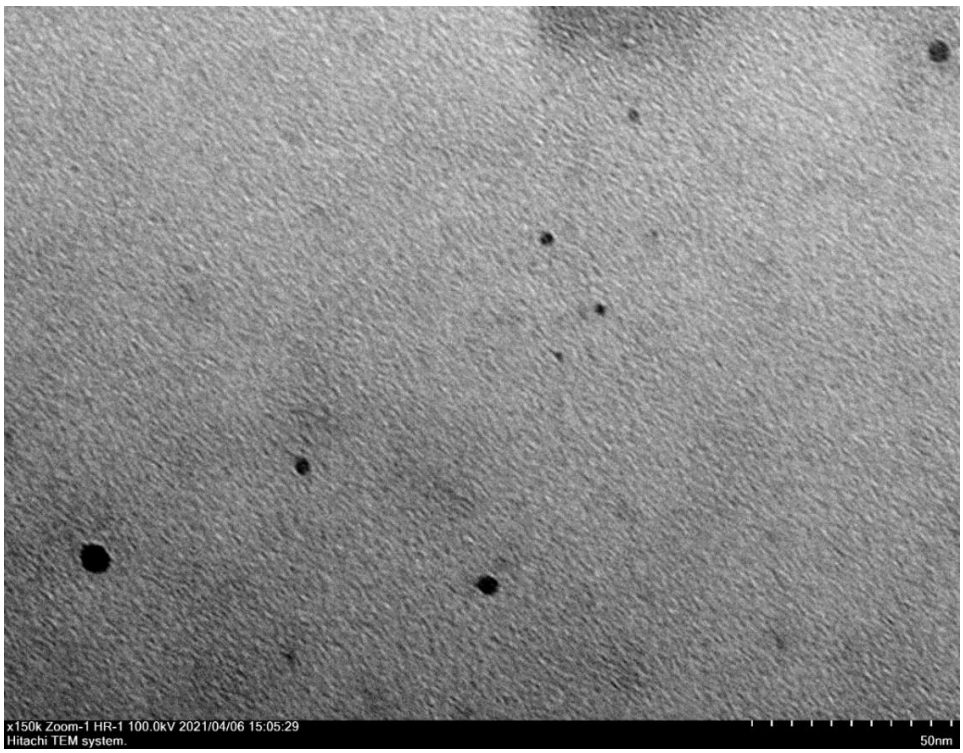

Figure S34. TEM image of Pt NPs from $HSiCl_3$ (**2a**) and Ph_2C_2 (**1a**) reaction supernatant in the presence of Pt/C.

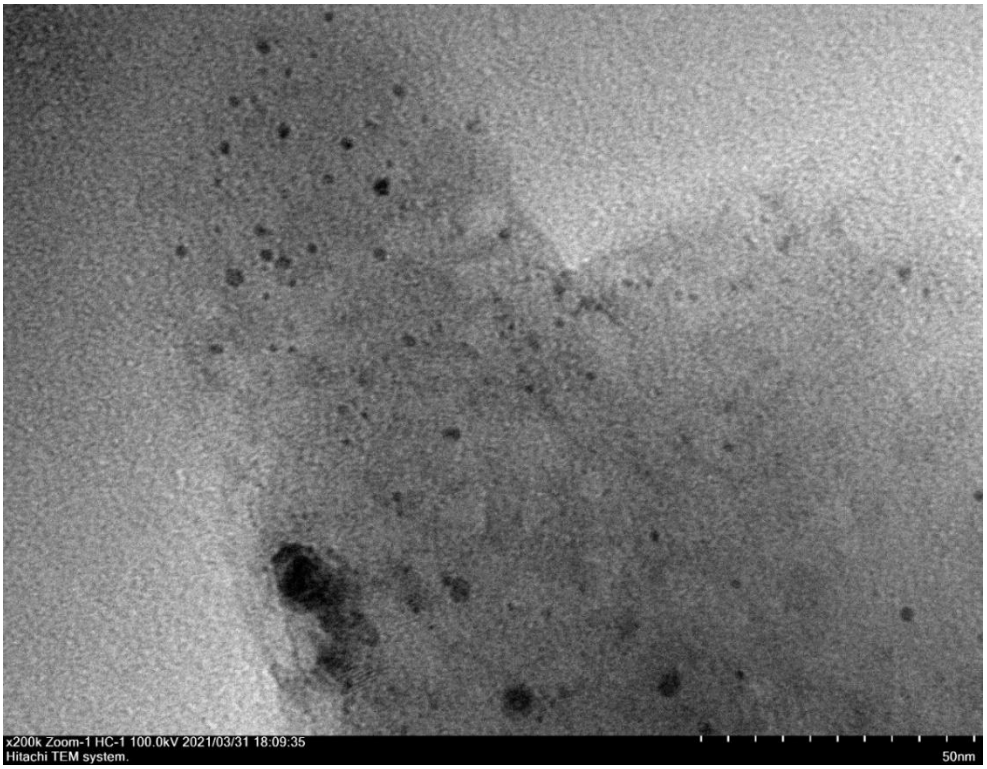

Figure S35. TEM image of Pt NPs from $HSiEt_3$ (**2b**) and Ph_2C_2 (**1a**) reaction supernatant in the presence of Pt/C.

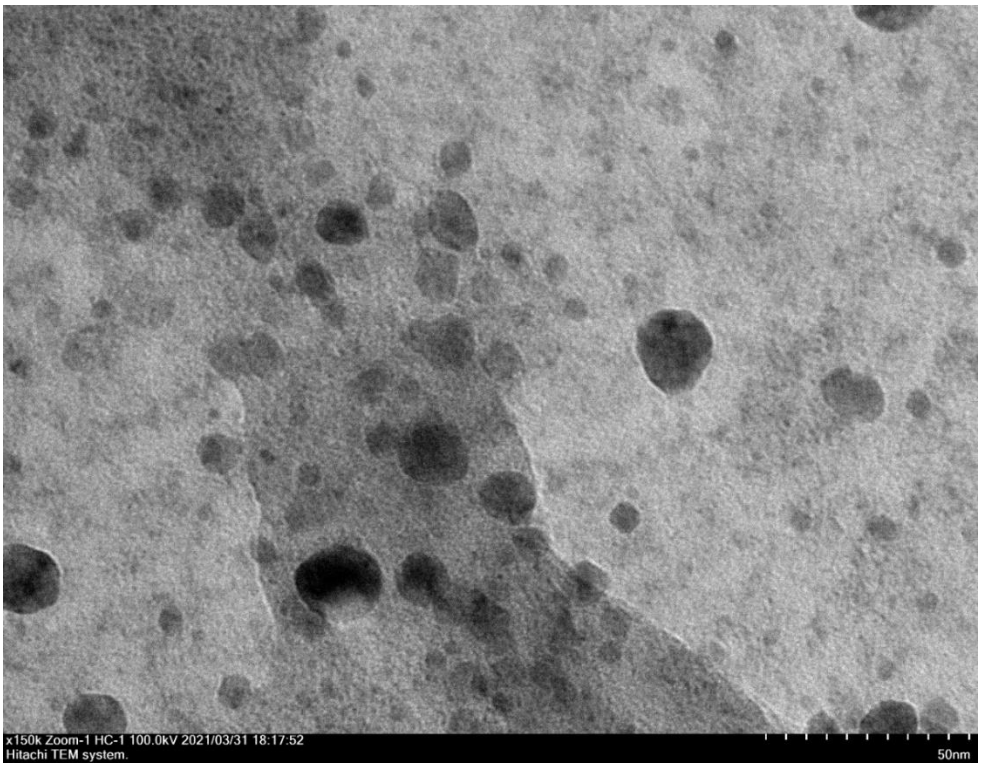

Figure S36. TEM image of Pt NPs from $HSiPh_3$ (**2c**) and Ph_2C_2 (**1a**) reaction supernatant in the presence of Pt/C.

Platinum nanoparticles size distribution histograms

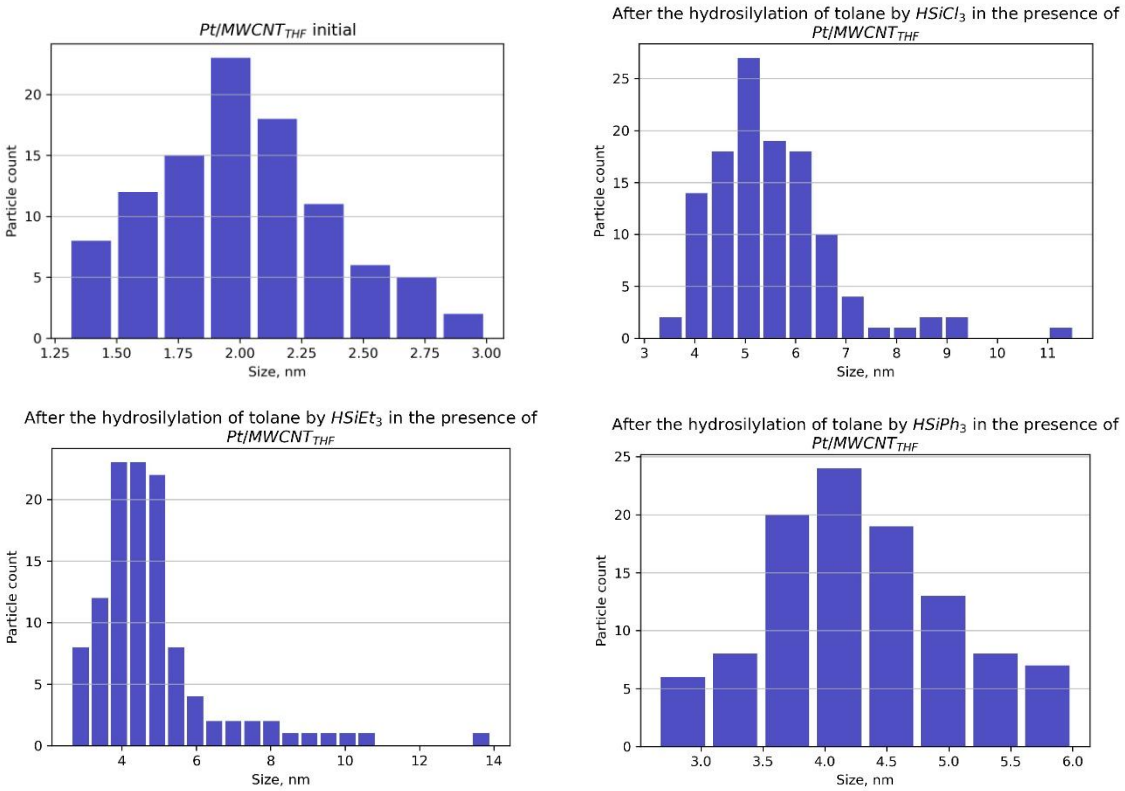

Figure S37. Size distribution histograms of Pt nanoparticles on Pt/MWCNT$_{THF}$ before and after model reaction with different silanes.

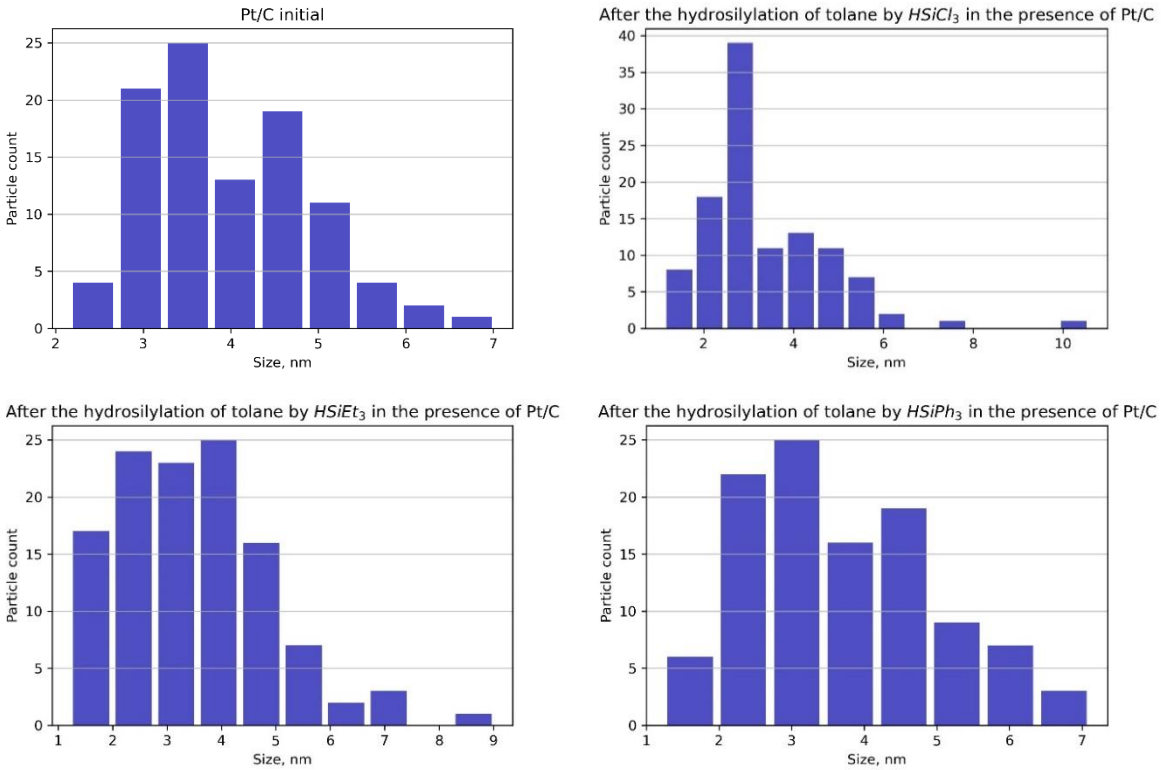

Figure S38. Size distribution histograms of Pt nanoparticles on Pt/C before and after model reaction with different silanes.

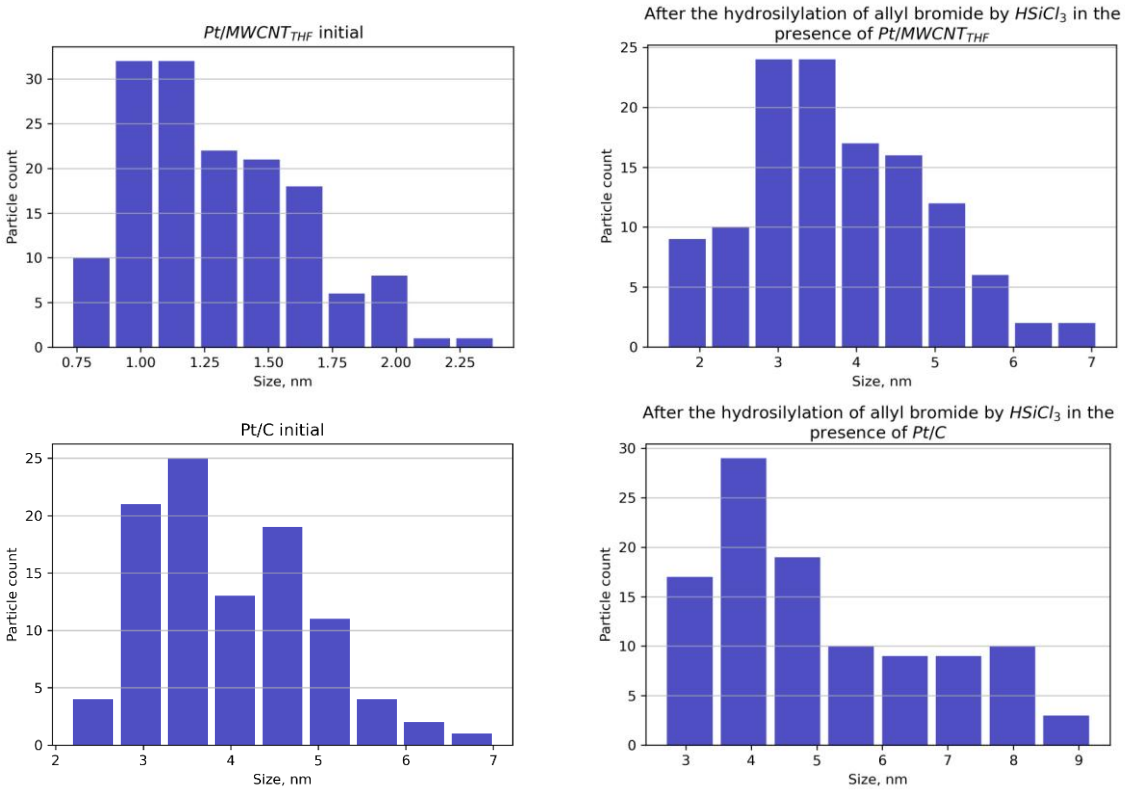

Figure S39. Size distribution histograms of Pt nanoparticles on Pt/MWCNT$_{THF}$ and Pt/C before and after allyl bromide hydrosilylation with $HSiCl_3$.

Hydrosilylation of tolane in the presence of Pt_2dba_3

A comparative study on the catalytic activity of the Pt_2dba_3 complex and premixed system was carried out. In four separate experiments, $Pt/MWCNT_{THF}$, Pt_2dba_3 with MWCNT, Pt_2dba_3, and MWCNT were used as catalysts in the model reaction (Table S4).

Table S4. Model reaction in the presence of the Pt_2dba_3

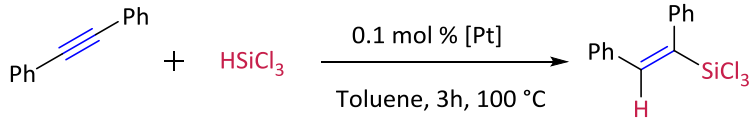

1a **2a** ***E*-3aa**

Entry	Catalyst	Yield, % [a]
1	$Pt/MWCNT_{THF}$	42
2	Pt_2dba_3 , MWCNT	77
3	Pt_2dba_3	98
4	MWCNT	0

[a] Yield of the products were determined by GC-MS.

Pt_2dba_3 and Pt_2dba_3, MWCNT worked as homogeneous catalysts (entries 2 and 3, Table S4) and gave yields higher than heterogeneous $Pt/MWCNT_{THF}$.

Characterization data

Table S5. Numbering of products of Pt/MWCNT$_{THF}$- and Pt/C-catalyzed hydrosilylation of internal alkynes using different silanes. Reaction conditions are summarized in Table S1**.**

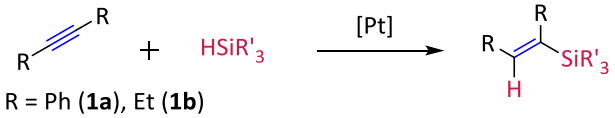

R = Ph (**1a**), Et (**1b**)
R' = Cl (**2a**), Et (**2b**), Ph (**2c**)

***E*-3**

Entry	Alkyne, R	Silane, R'	Product
1	Ph	Cl	**3aa**
2	Et		**3ba**
3	Ph	Et	**3ab**
4	Et		**3bb**
5	Ph	Ph	**3ac**
6	Et		**3bc**

Table S6. Numbering of products of Pt/MWCNT$_{THF}$- and Pt/C-catalyzed hydrosilylation of terminal alkynes using different silanes. Reaction conditions are summarized in Table S1.

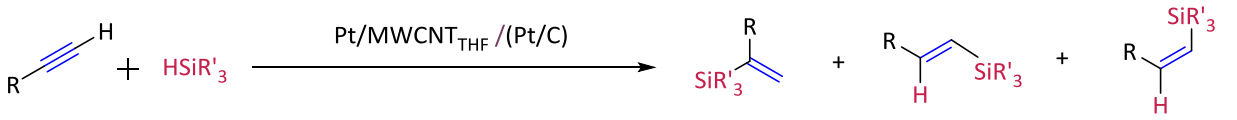

R = Ph (**1c**), n-Bu (**1d**), TMS (**1e**)
R' = Cl (**2a**), Et (**2b**), Ph (**2c**)

α-isomer (**3**) β-***E***-isomer (**4**) β-***Z***-isomer (**5**)

Entry	Alkyne	Silane	Product distribution, %	
			Pt/MWCNT$_{THF}$	Pt/C
	R	R'	**3 : 4 : 5**	**3 : 4 : 5**
1	Ph	Cl	**4ca**	**4ca**
2	n-Bu		**4da**	**4da**
3	TMS		**4ea**	**4ea**
4	Ph	Et	**3cb : 4cb**	**3cb : 4cb**
5	n-Bu		**3db : 4db : 5db**	**3db : 4db : 5db**
6	TMS		**3eb:4eb**	**3eb:4eb**
7	TMS	Ph	**3ec:4ec**	**3ec:4ec**

The obtained vinylsilanes were identified by ^{1}H and ^{13}C{^{1}H} NMR according to the published data for **3aa**,[3] **3ba**,[3] **3ab**,[3] **3bb**,[3] **3cb**,[3] **3db**,[3] **4ca**,[3] **4cb**,[3] **4da**,[3] **4db**,[3] **4ea**,[3] **4eb**,[3] **3ec**,[4] **4ec**,[4] **3ac,**[5] **3eb,**[6] **5db**[7]. All products were also checked by GC-MS (EI). Spectral data for **4bc** were not found in the literature, and the characterization is provided below.

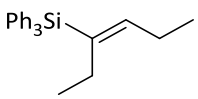

(E)-hex-3-en-3-yltriphenylsilane (**3bc**). Yield: 57 %.

^{1}H NMR (300 MHz, CDCl3): δ 7.75 – 7.57 (m, 6H), 7.57 – 7.34 (m, 9H), 6.05 (t, J = 7.0 Hz, 1H), 2.35 (dt, J = 8.7, 7.5 Hz, 4H), 1.09 (t, J = 7.5 Hz, 3H), 0.84 (t, J = 7.5 Hz, 3H). ^{13}C{^{1}H} NMR (75 MHz, CDCl3): δ 148.83, 136.45, 135.98, 135.06, 130.20, 129.30, 128.00, 127.72, 23.20, 22.22, 14.87, 14.14. GC-EI, m/z (relative intensity): 342 [M+, 261], 313(100), 264 (227), 260 (249), 259 (999), 235 (184), 183 (294), 181 (284), 180 (101), 105 (117).

References

1 E. O. Pentsak and V. P. Ananikov, *Russ. Chem. Bull.*, 2014, **63**, 2560–2563.

2 C. G. Baumann, S. De Ornellas, J. P. Reeds, T. E. Storr, T. J. Williams and I. J. S. Fairlamb, *Tetrahedron*, 2014, **70**, 6174–6187.

3 M. Chauhan, B. J. Hauck, L. P. Keller and P. Boudjouk, *J. Organomet. Chem.*, 2002, **645**, 1–13.

4 J. Fotie, M. Enechojo Agbo, F. Qu and T. Tolar, *Tetrahedron Lett.*, 2020, **61**, 152300.

5 A. Rivera-Hernández, B. J. Fallon, S. Ventre, C. Simon, M.-H. Tremblay, G. Gontard, E. Derat, M. Amatore, C. Aubert and M. Petit, *Org. Lett.*, 2016, **18**, 4242–4245.

6 X. Zhang, X. Ji, X. Xie and S. Ding, *Chem. Commun.*, 2018, **54**, 12958–12961.

7 X. Zhao, D. Yang, Y. Zhang, B. Wang and J. Qu, *Org. Lett.*, 2018, **20**, 5357–5361.